RESEARCH

Optimizing network neuroscience computation of individual differences in human spontaneous brain activity for test-retest reliability

Chao Jiang[1], Ye He[2], Richard F. Betzel[3], Yin-Shan Wang[4,5], Xiu-Xia Xing[6], and Xi-Nian Zuo[4,5,7,8]

[1]School of Psychology, Capital Normal University, Beijing, China
[2]School of Artificial Intelligence, Beijing University of Posts and Telecommunications, Beijing, China
[3]Department of Psychological and Brain Sciences, Indiana University, Bloomington, Indiana, USA
[4]State Key Laboratory of Cognitive Neuroscience and Learning, Beijing Normal University, Beijing, China
[5]Developmental Population Neuroscience Research Center, International Data Group/McGovern Institute for Brain Research, Beijing Normal University, Beijing, China
[6]Department of Applied Mathematics, College of Mathematics, Faculty of Science, Beijing University of Technology, Beijing, China
[7]National Basic Science Data Center, Beijing, China
[8]Institute of Psychology, Chinese Academy of Sciences, Beijing, China

ABSTRACT

A rapidly emerging application of network neuroscience in neuroimaging studies has provided useful tools to understand individual differences in intrinsic brain function by mapping spontaneous brain activity, namely intrinsic functional network neuroscience (ifNN). However, the variability of methodologies applied across the ifNN studies—with respect to node definition, edge construction, and graph measurements—makes it difficult to directly compare findings and also challenging for end users to select the optimal strategies for mapping individual differences in brain networks. Here, we aim to provide a benchmark for best ifNN practices by systematically comparing the measurement reliability of individual differences under different ifNN analytical strategies using the test-retest design of the Human Connectome Project. The results uncovered four essential principles to guide ifNN studies: (1) use a whole brain parcellation to define network nodes, including subcortical and cerebellar regions; (2) construct functional networks using spontaneous brain activity in multiple slow bands; and (3) optimize topological economy of networks at individual level; and (4) characterize information flow with specific metrics of integration and segregation. We built an interactive online resource of reliability assessments for future ifNN (https://ibraindata.com/research/ifNN).

AUTHOR SUMMARY

It is an essential mission for neuroscience to understand the individual differences in brain function. Graph or network theory offer novel methods of network neuroscience to address such a challenge. This article documents optimal strategies on the test-retest reliability of measuring individual differences in intrinsic brain networks of spontaneous activity. The analytical pipelines are identified to optimize for highly reliable, individualized network measurements. These pipelines optimize network metrics for high interindividual variances and low inner-individual variances by defining network nodes with whole-brain parcellations, deriving the connectivity with spontaneous high-frequency slow-band oscillations, constructing brain graphs with topology-based methods for edge filtering, and favoring

multilevel or multimodal metrics. These psychometric findings are critical for translating the functional network neuroscience into clinical or other personalized practices requiring neuroimaging markers.

INTRODUCTION

Over the past two decades, network neuroscience has helped transform the field of neuroscience (D. Bassett et al., 2020), providing a quantitative methodology framework for modeling brains as graphs (or networks) composed of nodes (brain regions) and edges (their connections), namely connectomics (Sporns, 2013a). The organization and topology of macroscale brain networks can be characterized by a growing suite of connectomic measurements including efficiency, centrality, clustering, small-word topology, rich-club, and so forth (Craddock et al., 2013). In parallel, resting-state fMRI (rfMRI) has opened up new avenues toward understanding the intrinsic human brain function (Biswal et al., 2010). In conjunction with network neuroscience, rfMRI has led to the emergence of a multidisciplinary field, intrinsic functional connectomics or network neuroscience (ifNN), in which the brain's intrinsic, interregional connectivity is estimated from rfMRI recordings. It has been widely used to investigate the system-level organization of the human brain function and its relationship with individual differences (Dubois & Adolphs, 2016) in developmental (Zuo et al., 2017), sociocultural (Pessoa, 2018), and clinical conditions (Fornito, Zalesky, & Breakspear, 2015).

Highly reliable measurements are essential for studying individual differences. In general, reliability characterizes a proportion of measurement variability between different subjects relative to the overall variability including both between-subject and within-subject (i.e., random) components (Xing & Zuo, 2018). It is commonly used to assess the consistency or agreement between measurements, or the ability to obtain consistent measures over time. Beyond that, it can also serve as a measure of discriminability (Xing & Zuo, 2018; Zuo, Biswal, & Poldrack, 2019a; Zuo, Xu, & Milham, 2019b). For example, if a measurement can more sufficiently capture individual characteristics (i.e., better differentiate a group of individuals), it will produce higher between-subject variability and thus higher reliability than a measurement underestimating the between-subject variability. Such reliability concept has well-established statistical theory and applications in fields such as psychology (Elliott, Knodt, Caspi, Moffitt, & Hariri, 2021a) and medicine (Kraemer, 2014) where it is used in psychometric theory and diagnosis theory, respectively. Specifically, in psychology, reliability is important for assessing the validity of psychological tests, and in medicine, it is important for accurately diagnosing and treating patients. In the field of human brain mapping, more recent studies have demonstrated that the measurement reliability is equivalent to the "fingerprint" or discriminability of the measurement under the Gaussian distribution (Bridgeford et al., 2021; Milham, Vogelstein, & Xu, 2021). Therefore, the optimization of measurement reliability of the individual differences can help guide ifNN processing and analysis pipelines for individualized or personalized (e.g., neurodevelopmental; Herting, Gautam, Chen, Mezher, & Vetter, 2018) or clinical (Matthews & Hampshire, 2016) research.

Previous studies have demonstrated that many functional network measurements with rfMRI have limited reliability (Noble, Scheinost, & Constable, 2019; Zuo & Xing, 2014). These low levels of reliability could be an indication of failure in handling individual variability at different levels (Elliott, Knodt, & Hariri, 2021b; Hallquist & Hillary, 2019). In particular, experimental design and processing decisions related to scan duration, determining frequency

Brain topology:
A quantitative description on structural and functional relationships of the brain organization and their links to mind.

Resting state:
A paradigm in neuroimaging developed to approch the balance state of brain as a complex system from a perspective of dynamic physics, commonly a state of lying-down quietly without systematic or specific thoughts.

Measurement reliability:
Proportion of between-subject variability of a measurement relative to its overall variability including both between-subject and within-subject components.

Parcellation:
A division into parcels defining distinct partitions of neural elements in the brain.

range, and regressing global signal have impacts on rfMRI measurements and thus their reliability (Noble et al., 2019; Zuo et al., 2013). Although less focused on reliability, existing network neuroscience studies revealed that their findings are influenced by choices of parcellation templates (Bryce et al., 2021; Wang et al., 2009), edge construction and definition, and choice of graph metrics (Liang et al., 2012). How these decisions affect the measurement reliability in ifNN deserves further investigation. These analytical choices have been implemented in different software packages but can vary from one package to another, and thus introduce more analytic variability (Botvinik-Nezer et al., 2020). Beyond limited examinations on reliability (Aurich, Filho, da Silva, & Franco, 2015; Braun et al., 2012; Termenon, Jaillard, Delon-Martin, & Achard, 2016), a systematic investigation into the measurement reliability is warranted to guide ifNN software use and analyses.

We conducted a systematic ifNN reliability analysis using the test-retest rfMRI data from the Human Connectome Project (HCP). The HCP has developed its imaging acquisition and data preprocessing (Glasser et al., 2013) by integrating various strategies optimized for reliability in previous studies (Noble et al., 2019; Noble, Scheinost, & Constable, 2021; Zuo & Xing, 2014; Zuo et al., 2013). We thus analyzed the minimally preprocessed HCP rfMRI data and focused our work on four key postanalytic stages: node definition, edge construction, network measurement, and reliability assessments. In the end, we propose a set of principles to guide researchers in performing reliable ifNN, advancing the fieldstandard call for the best practices in network neuroscience. We released all the codes and reliability data by building an online platform for sharing the data and computational resources to foster future ifNN.

THEORY AND METHODS

A typical analysis pipeline in ifNN includes steps for node definition (parcellations) and edge construction (frequency bands, connectivity estimation and filtering schemes) (Figure 1A). To determine an optimal pipeline, we combine the most reliable strategies across different parts of the analysis by comparing the reliability of derived global network metrics. The HCP test-retest data were employed for reliability evaluation (Figure 1B) using the intraclass correlation (ICC) statistics on the measurement reliability. Overall reliability assessments associated with the various analytic strategies as well as their impact on between- and within-subject variability (Figure 1C) are investigated. We calculated the between-subject variability (V_b) and within-subject variability (V_w) and normalized them to values between 0 and 1 by the total sample variances. The changes in these variability measures, ΔV_b and ΔV_w were used to create a reliability gradient represented by a vector. The length of the arrow reflects the amplitude of the change in reliability when comparing one choice (pink circle, *J*) to another choice (red circle, *K*). The direction of the arrow, **JK**, indicates the sources of the change in reliability. In this case, the reliability increases from a moderate to a substantial level with an increase in between-subject variability ($\Delta V_b > 0$) and a decrease in within-subject variability ($\Delta V_w < 0$). We then determine the optimized pipelines based on the highest reliability measurements, while documenting the derived both global and local network metrics and both their reliability and variability at an individual level. We first introduce the reliability theory and assessments.

Reliability Theory and Assessments

Measurement reliability is defined as the extent to which measurements can be replicated across multiple repeated measuring occasions (Xing & Zuo, 2018; Zuo, Biswal, & Poldrack,
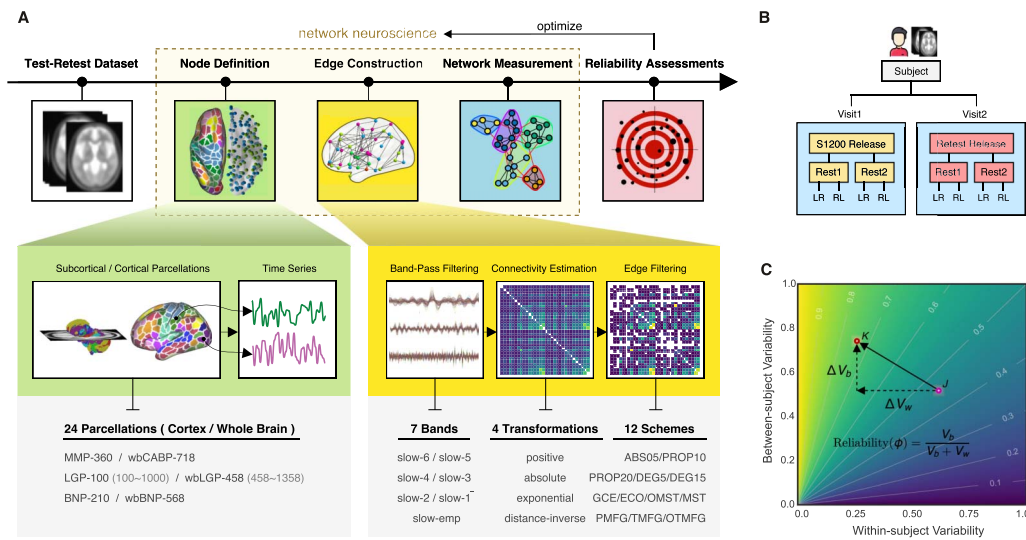
Figure 1. Analytical pipelines for reliable ifNN. (A) There are five stages during our analyses: (1) test-retest dataset (white box) downloaded from HCP website; (2) node definition (green box) defining nodes using a set of brain areas of 24 different partitions of the human brain; (3) edge construction (yellow box) estimating individual correlation matrices using the six frequency bands (slow 1–6) from Buzsaki's theoretical framework on the brain oscillations as well as the widely used empirical frequency band (Slow-emp) and transferring these matrices into adjacency matrices using 7 × 4 × 12 different strategies on edge construction including band-pass filtering, connectivity estimation and edge filtering; (4) network analysis (blue box) systematically calculating various brain graph metrics on measurements of information flow; and (5) reliability assessment (red box) evaluating test-retest reliability with massive linear mixed models. (B) The test-retest data shared multimodal MRI datasets of 46 subjects in the HCP S1200 release and the HCP Retest release. Each subject underwent the first four test scans on 2 days (two scans per day: Rest1 and Rest2) and return several months later to finish the four retest scans on another 2 days. (C) Measurement reliability refers to the interindividual or between-subject variability V_b relative to the intraindividual or within-subject variability V_w. Variability of both between-subject (V_b) and within-subject (V_w) are normalized into between 0 and 1 by the total sample variances. Their changes (ΔV_b and ΔV_w) introduce a reliability gradient as represented by the vector (the black arrow). The length of the arrow reflects the amplitude of reliability changes when the reliability assessment from one choice (pink circle, J) to another choice (red circle, K). Further, the arrow's direction (**JK**) indicates the sources of this reliability change. Here the reliability becomes from moderate to substantial level with increases of between-subject variability ($\Delta V_b > 0$) and decreases of within-subject variability ($\Delta V_w < 0$).

2019a; Zuo, Xu, & Milham, 2019b). Test-retest reliability is the closeness of the agreement between the results of successive measurements of the same measure and carried out under the same conditions of measurement.

Linear mixed models. As a group-level statistic, reliability refers to the interindividual or between-subject variability V_b relative to the intraindividual or within-subject variability V_w. Both the intra- and inter-individual variances can be estimated using linear mixed model (LMM). In this study, given a functional graph metric ϕ, we considered a random sample of P subjects with N repeated measurements of a continuous variable in M visits. ϕ_{ijk} (for $i = 1, ..., N$ and $j = 1, ..., M$, and $k = 1, ..., P$) denotes the metric from the kth subject's j^{th} visit and i^{th} measurement occasions. The three-level LMM models ϕ_{ijk} as the following equations:

$$\underbrace{\phi_{ijk}}_{\text{Graph metric}} = \underbrace{\gamma_{000}}_{\substack{\text{fixed} \\ \text{intercept}}} + \underbrace{p_{0k}}_{\substack{\text{random intercepts} \\ \text{level 3, subjects}}} + \underbrace{v_{0jk}}_{\substack{\text{random intercepts} \\ \text{level 2, visits}}} + \underbrace{e_{ijk}}_{\substack{\text{random} \\ \text{residuals}}}$$

where γ_{000} is a fixed parameter (the group mean) and p_{0k}, v_{0jk}, and e_{ijk} are independent random effects normally distributed with a mean of 0 and variances σ_{p0}^2, σ_{v0}^2, and σ_e^2. The term p_{0k} is the subject effect, v_{0jk} is the visit effect, and e_{ijk} is the measurement residual. Age, gender, and interval (Δt) between two visits are covariants.

ICC estimation. These variances are used to calculate the test-retest reliability, which is measured by the dependability coefficient and reflects the absolute agreement of measurements. The dependability coefficient is a form of ICC commonly, which is the ratio of the variances due to the object of measurement versus sources of error. To avoid negative ICC values and obtain more accurate estimation of the sample ICC, the variance components in model are usually estimated with the restricted maximum likelihood approach with the covariance structure of an unrestricted symmetrical matrix (Zuo et al., 2013).

$$\text{Reliability}\,(\phi) = \frac{V_b}{V_b + V_w} = \frac{\sigma_{p0}^2}{\sigma_{p0}^2 + \sigma_e^2} \tag{ICC}$$

The ICC statistics on the measurement reliability are categorized into five common levels: $0 < \text{ICC} \leq 0.2$ (**slight**); $0.2 < \text{ICC} \leq 0.4$ (**fair**); $0.4 < \text{ICC} \leq 0.6$ (**moderate**); $0.6 < \text{ICC} \leq 0.8$ (**substantial**); and $0.8 < \text{ICC} < 1.0$ (**almost perfect**). A metric with moderate to almost perfect test-retest reliability (ICC ≥ 0.4) is commonly expected in practice. The ICC level should not be judged only based upon the point statistical estimation of ICC but its confidence intervals (CI) (Koo & Li, 2016). We employed the nonparametric conditional bootstrap method for 1,000 times to estimate their 95% CIs.

Statistics evaluation. Our analyses can produce big data of 524,160 ICCs (419,328 for the global network metrics). These ICCs are grouped into four categories (parcellation, frequency band, connectivity transformation, and edge filtering scheme), each of which has different choices. Given each choice of a category, we estimated its density distributions of ICCs and calculated two descriptive statistics: (1) mean ICC values, which measures the *general reliability* under the given choice; (2) number of almost perfect (noap) ICC values, which measures the *potential reliability* under the given choice.

We further perform Friedman rank sum test to evaluate whether the location parameters of the distribution of ICCs are the same in each choice. Once the Friedman test is significant, we employ the pairwise Wilcoxon signed rank test for post hoc evaluations to compare ICCs between each pair of the distributions under different choices. The statistical significance levels are corrected with Bonferroni method for controlling the familywise error rate at a level of 0.05. We develop a method to visualize and evaluate the change of ICCs (i.e., reliability gradient) between different choices (Figure 1C). Specifically, the reliability can be plotted as a function of V_b and V_w in its anatomy plane (Xing & Zuo, 2018; Zuo, Xu, & Milham, 2019b). The gradient of reliability between two choices is modeled by the vector (i.e., the black arrow), and decomposed into changes of individual variability. The systematic evaluation on the reliability of the global network metrics determines the optimal network neuroscience by combining the most reliable pipeline choices, which further generated the nodal metrics' reliability.

Specifically, using the HCP test-retest dataset, our analytic procedure implemented the four postanalytic stages: node definition, edge construction, network measurement, and reliability assessments. The test-retest rfMRI dataset underwent the standardized preprocessing pipeline developed by the HCP team (Glasser et al., 2013). The second step defines nodes (green box) using sets of brain areas based on 24 partitions, and then extracts the nodal time series. During the third step (yellow box), individual correlation matrices are first estimated based upon the six frequency bands derived from Buzsaki's theoretical framework on brain oscillations (Buzsaki & Draguhn, 2004) along with the classical band widely used (0.01–0.08 Hz). These matrices are then converted into adjacency matrices using $4 \times 12 = 48$ strategies on edge filtering. In the fourth step, we performed graph analyses (blue box) by systematically calculating the brain graph metrics at global, modular, and nodal scales. Finally, test-retest reliability

was evaluated (red box) as ICCs with the linear mixed models as described above. We present details of the other three stages of analyses in the following sections.

Test-Retest Dataset

The WU-Minn Consortium in HCP shared a set of test-retest multimodal MRI datasets of 46 subjects from both the S1200 release and the Retest release. These subjects were retested using the full HCP 3T multimodal imaging and behavioral protocol. Each subject underwent the four scans on 2 days (two scans per day: Rest1 versus Rest2) during the first visit and returned several months later to finish the four scans on another two days during the second visit (Figure 1B). The test-retest interval ranged from 18 to 328 days (mean: 4.74 months; standard deviation: 2.12 months). Only 41 subjects (28 females, age range: 26–35 years; 13 males, age range: 22–33 years) had full length rfMRI data across all the eight scans, 2 visits × 2 days × 2 (LR and RL encoding directions), and were included in the subsequent analyses. Then we averaged across the RL and LR encodings for each day, so each subject had four repeated measurements in the ICC estimation. This sample size is larger than the minimal sample size ($N = 35$) for fair reliability with 80% power and significance level of 0.05 based on the above-mentioned test-retest design (four observations per subject) (Bujang & Baharum, 2017). The HCP rfMRI protocols for scanning and preprocessing images have been optimized for reliability.

During the scanning, participants were instructed to keep their eyes open and to let their mind wander while fixating on a cross-hair projected on a dark background. Data were collected at the 3T Siemens Connectome Skyra MRI scanner with a 32-channel head coil. All functional images were acquired using a multiband gradient-echo EPI imaging sequence (2 mm isotropic voxel, 72 axial slices, TR = 720 ms, TE = 33.1 ms, flip angle = 52°, field of view = 208 × 180 mm^2, matrix size = 104 × 90 and a multiband factor of 8). A total of 1,200 images was acquired for a duration of 14 min and 24 s. Details on the imaging protocols can be found in Smith et al. (2013).

The protocols of rfMRI image preprocessing and artifact removal procedures are documented in detail elsewhere and generated the minimally preprocessed HCP rfMRI images. Artifacts were removed using the ICA-based X-noiseifier (ICA + FIX) procedure, followed by MS-MAll for intersubject registration. The preprocessed rfMRI data were represented as a time series of grayordinates (4D), combining both cortical surface vertices and subcortical voxels (Glasser et al., 2013).

Node Definition

Brain graph:
A mathematical abstract using graph thery to define a brain system as a set of nodes and interconnecting edges.

A brain graph defines a node as a brain area, which is generally derived by an element of brain parcellation (parcel) according to borders or landmarks of brain anatomy, structure, or function as well as an element of volume (voxel) in imaging signal acquisition or a cluster of voxels (Sporns, 2013b). Due to the high computational demand of voxel-based brain graph, in this study, we defined nodes as parcels according to the following brain parcellation strategies (Figure 2A). A surface-based approach has been demonstrated to outperform other approaches for fMRI analysis (Coalson, Van Essen, & Glasser, 2018; Zuo et al., 2013), and thus the nodes are defined in the surface space (total 24 surface parcellation choices). Of note, we adopted a naming convention for brain parcellations as follows: *ParcAbbr-NumberOfParcels'* (e.g., LGP-100 or its whole-brain version wbLGP-458).

HCP multimodal parcellation (MMP). A cortical parcellation generated from multimodal images of 210 adults from the HCP database, using a semiautomated approach (Glasser et al., 2016).
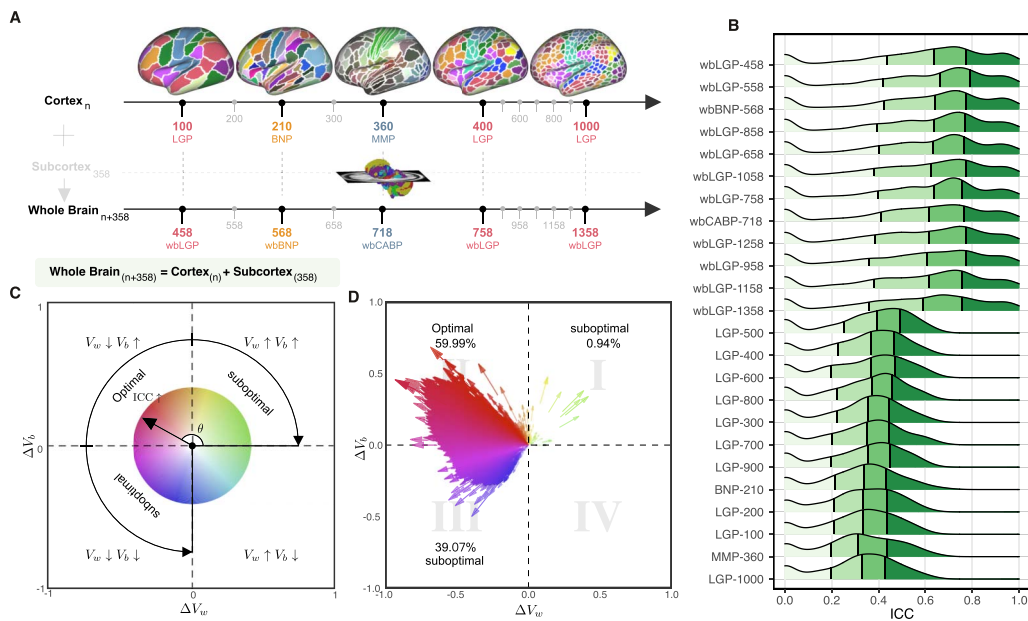
Figure 2. Parcellation choices impact measurement reliability and individual variability. (A) Node definitions are derived from the process of spatially partitioning the human cortex and whole brain (including both cortical and subcortical nodes) at various resolutions; see more details of these name abbreviations in Theory and Methods. (B) Density plots are visualized for distributions of the ICCs under the various parcellation choices on node definition. These density distributions are ranked from top to bottom according to decreases of the mean ICCs while the four colors depict the four quantiles. (C) Reliability gradient between any one whole-brain parcellation choice and its corresponding cortical parcellation choice is decomposed into the axis of changes of the between-subject variability (ΔV_b) and the axis of changes of the within-subject variability (ΔV_w). This gradient can be represented as a vector, which is the black arrow from the origin with an angle θ with the x axis, while the color encodes this angle and the transparency or the length reflects the magnitude of the degree of ICC improvement. According to the anatomy of reliability, the optimal space is in the second quadrant (quadII) while the first and third quadrant (quadI and quadIII) are suboptimal for reliability. (D) The improvement in the reliability of the pipeline, which is defined from the cortical parcellations to the corresponding whole-brain parcellations (including the subcortex), is illustrated by gradient arrows in the plane of individual variability, while controlling for all other processing steps. Each arrow represents a specific global metric, while controlling for all other processing steps. The position of the arrows reflects the magnitude of between- and within-subject variability changes (ΔV_b, ΔV_w), and the size of the arrows indicates the magnitude of ICC changes.

Cortical regions are delineated with respect to their function, connectivity, cortical architecture, and topography, as well as expert knowledge and meta-analysis results from the literature (Glasser et al., 2016). The atlas contains 180 parcels for each hemisphere.

Local-global parcellation (LGP). A gradient-weighted Markov random field model integrating local gradient and global similarity approaches produces the novel parcellations (Schaefer et al., 2018). The final version of LGP comes with a multiscale cortical atlas including 100, 200, 300, 400, 500, 600, 700, 800, 900, and 1,000 parcels (equal numbers across the two hemispheres). One benefit of using LGP is to have nodes with almost the same size, and these nodes are also assigned to the 4acommon large-scale functional networks (Thomas Yeo et al., 2011).

Brainnetome parcellation (BNP). Both anatomical landmarks and connectivity-driven information are employed to develop this volumetric brain parcellation (Fan et al., 2016). Specifically, anatomical regions defined as in Desikan et al. (2006) are parcellated into subregions using functional and structural connectivity fingerprints from HCP datasets. Cortical parcels are obtained by projecting their volume space to surface space. It is noticed that the original BNP contains both cortical (105 areas per hemisphere) and subcortical (36 areas) regions but only the 210 cortical parcels are included for the subsequent analyses.

Whole-brain parcellation (wb). Inclusion of subcortical areas has been shown to contain unignorable influences on brain graph analyses (D. Greene et al., 2020; Noble et al., 2019), and we thus also constructed brain graphs with subcortical structures in volume space as nodes by adding these nodes to the cortical brain graphs. To get a high-resolution subcortical parcellation, we adopted the 358 subcortical parcels in Ji et al. (2019). The authors employed data of 337 unrelated HCP healthy volunteers and extended the MMP cortical network partition into subcortex. This results in a set of whole-brain parcellations by combining these subcortical parcels with the aforementioned cortical parcellations, namely **wbMMP**, **wbLGP**, and **wbBNP**. We noticed that the wbMMP-718 has been named by Ji et al. (2019) as the Cole-Anticevic Brain-wide Network Partition, and we thus renamed the wbMMP-718 as wbCABP-718 for consistency.

Edge Construction

After defining the node with each parcellation, in each parcel, regional mean time series were estimated by averaging the vertex time series at each time point. To construct an edge between a pair of nodes, their representative time series entered into the following steps in order: *band-pass filtering, internode connectivity transformation*, and *edge filtering*.

Band-pass filtering. Resting-state functional connectivity studies have typically focused on fluctuations below 0.08 Hz or 0.1 Hz (Biswal, Zerrin Yetkin, Haughton, & Hyde, 1995; Fox & Raichle, 2007) and assumed that only these frequencies contribute significantly to interregional functional connectivity while other frequencies are artifacts (Cordes et al., 2001). In contrast, however, other studies have found that specific frequency bands of the rfMRI oscillations make unique and neurobiologically meaningful contributions to resting-state functional connectivity (Salvador et al., 2005; Zuo & Xing, 2014). More recently, with fast fMRI methods, some meaningful FC patterns were reported across much higher frequency bands (Boubela et al., 2013). These observations motivate exploring a range of frequency bands beyond those typically studied in resting-state functional connectivity studies.

Buzsaki and Draguhn (2004) proposed a hierarchical organization of frequency bands driven by the natural logarithm linear law. This offers a theoretical template for partitioning rfMRI frequency content into multiple bands (Figure 3A). The frequencies occupied by these bands have a relatively constant relationship to each other on a natural logarithmic scale and have a constant ratio between any given pair of neighboring frequencies (Buzsáki, 2009). These different oscillations are linked to different neural activities, including cognition, emotion regulation, and memory (Achard, Salvador, Whitcher, Suckling, & Bullmore, 2006; Buzsáki, 2009; Fox & Raichle, 2007). Advanced by the fast imaging protocols offered by the HCP scanner, the short scan interval (TR = 720 ms) allows us to obtain more oscillation classes that the traditional rfMRI method. We incorporate Buzsaki's framework (Buzsaki & Draguhn, 2004; Penttonen & Buzsáki, 2003) with the HCP fast-TR datasets by using the DREAM toolbox (Gong et al., 2021) in the Connectome Computation System (Xing, Xu, Jiang, Wang, & Zuo, 2022; Xu, Yang, Jiang, Xing, & Zuo, 2015). It decomposed the time series into the six slow bands as illustrated in Figure 3A.

Connectivity transformation. For each scan, individual nodal representative time series were band-pass filtered with each of the six frequency bands, and another empirical frequency band, slow-emp (0.01–0.08 Hz). The Pearson's correlation $r_{ij} \in [-1, 1]$ between the filtered time series of each pair of nodes $i = 1, ..., N, j = 1, ..., N$ was calculated (N is the number of nodes). These correlation values provided an estimation on the edge strengths between the two nodes and formed a $N \times N$ symmetric correlation matrix $R = (r_{ij})$ for each given subject, scan, parcellation, and frequency band.

Functional connectivity: Relationship defined by temporal dependency between two functional units (e.g., brain areas).

Natural logarithm linear law: A special case of power law to divide frequencies of brain oscillations into specific bands with relatively constant relationship to each other on a natural logarithmic scale and a constant ratio between any pair of neighboring bands.
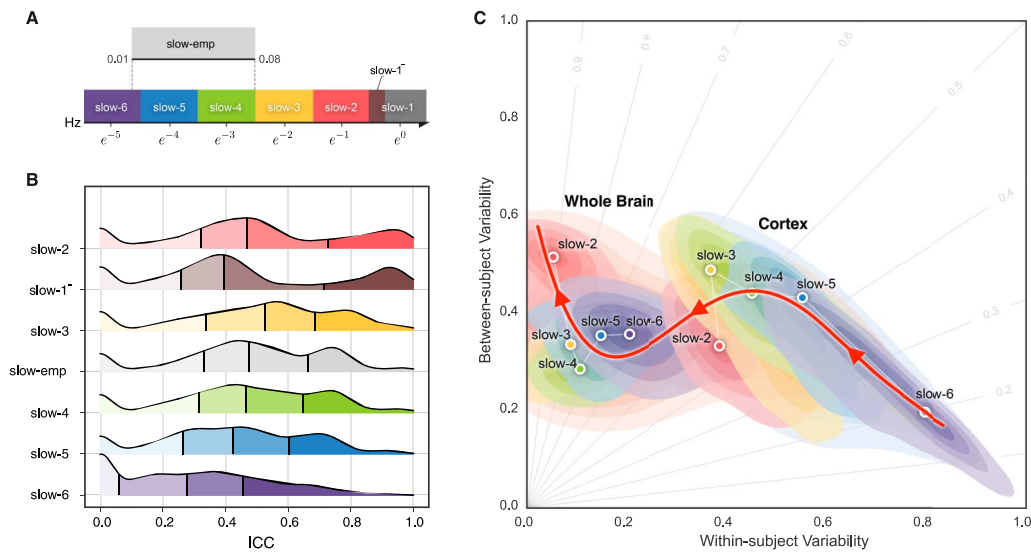
Figure 3. Reliability gradient across the slow bands and changes of related individual variability. (A) Classes of frequency bands for slow oscillations derived from the natural logarithm linear law. (B) Density plots are visualized for the ICC distributions under the various frequency bands. These density distributions are ranked from top to bottom according to decreases of the mean ICCs, while the vertical lines depict the four quartiles. (C) Network measurements are projected onto the reliability anatomy plane coordinated by both between- and within-subject variability. These dot plots are fitted into the topographic (contour) maps where the local maxima for each band is labeled as a circle. To highlight the trend of increasing reliability as the frequency band increases, a fourth-order polynomial curve (represented by a red line) is fitted to the frequency contour plot peak points, tracing the reliability flow along slow-to-fast oscillations in the cortex and whole brain.

Many network metrics are not well defined for negatively weighted connections. In order to ensure that the connection weights are positive only, we applied four types of transformations to the symmetric correlation matrix: the **positive** (Equation pos), **absolute** (Equation abs), **exponential** (Equation exp) and **distance-inverse** (Equation div) functions, respectively. This avoids the negative values in the internode connectivity matrix $W = (w_{ij})$ where $z_{ij} = \tanh^{-1}(r_{ij})$ is Fisher's z–transformation.

$$w_{ij} = \frac{z_{ij} + |z_{ij}|}{2} \in [0, \infty) \tag{pos}$$

$$w_{ij} = |z_{ij}| \in [0, \infty) \tag{abs}$$

$$w_{ij} = \mathbf{e}^{z_{ij}} \in [0, \infty) \tag{exp}$$

$$w_{ij} = \frac{2}{\sqrt{2 \times (1 - r_{ij})}} \in (0, \infty) \tag{div}$$

The connectivity matrix represents a set of the node parcels and relational quantities between each pair of the nodes, and will serve as the basis of following edge filtering procedure for generation of the final brain graphs.

Connectome:
A term describing the whole-brain graph and initiating the field of connectomics.

Edge filtering. In a graph, edges represent a set of relevant interactions of crucial importance to obtain parsimonious descriptions of complex networks. Filtering valid edges can be highly challenging due to the lack of 'ground truth' of the human brain connectome. To provide a

reliable way of building candidate edges, we sampled the following 12 schemes on edge filtering and applied them to the connectivity matrices.

Absolute weight thresholding (ABS). This approach selects those edges that exceed a manually defined absolute threshold (e.g., correlations higher than 0.5), setting all correlations smaller than 0.5 to 0 (ABS_{05}). This is a simple approach to reconstruct networks (Hagmann et al., 2007).

Proportional thresholding (PROP). It is a common step in the reconstruction of functional brain networks to ensure equal edge density across subjects (D. Bassett et al., 2009; Rubinov, Sporns, van Leeuwen, & Breakspear, 2009; van den Heuvel et al., 2017). It keeps the number of connections fixed across all individuals to rule out the influence of network density on the computation and comparison of graph metrics across groups. This approach includes the selection of a fixed percentage of the strongest connections as edges in each individual network or brain graph. Compared to ABS, PROP has been argued to reliably separate density from topological effects (Braun et al., 2012; Ginestet, Nichols, Bullmore, & Simmons, 2011) and to result in more stable network metrics (Garrison, Scheinost, Finn, Shen, & Constable, 2015). This makes it a commonly used approach for network construction and analysis in disease-related studies. Here, we focused on two thresholds that are commonly reported in the literature: 10% ($PROP_{10}$) and 20% ($PROP_{20}$).

Degree thresholding (DEG). The structure of a graph can be biased by the number of existing edges. Accordingly, statistical measures derived from the graph should be compared against graphs that preserve the same average degree, K. A threshold of the degree can be chosen to produce graphs with a fixed mean degree (e.g., $K = 5$, DEG_5), which is the average nodal degrees of an individual graph from a single subject's scan. Many network neuroscience studies have taken this choice for $K = 5$ (S. I. Dimitriadis, Laskaris, Del Rio-Portilla, & Koudounis, 2009; Micheloyannis et al., 2006; Milo et al., 2002; Stam, Jones, Nolte, Breakspear, & Scheltens, 2007). We also include the DEG_{15} for denser graphs of the brain networks.

Global cost efficiency optimization (GCE). Given a network with a cost ρ, its global efficiency is a function of the cost $E_g(\rho)$, and its GCE is $J(\rho) = E_g(\rho) - \rho$. Several studies suggested that brain networks, in particular those with small-world topology, maximize their global cost efficiency (D. S. Bassett et al., 2008), that is, $J^{max} = \max_\rho J(\rho)$. Computationally, this scheme is implemented by looping all network costs (e.g., adding edges with weights in order) to find the J^{max} where the corresponding edge weight was determined as the threshold for edge filtering. In this sense, GCE is an individualized and optimized version of ABS, PROP, and DEG, while the latter three are commonly employed with a fixed threshold for all individuals.

Overall efficiency cost optimization (ECO). Both global and local efficiency are important graph features to characterize the structure of complex systems in terms of integration and segregation of information (Latora & Marchiori, 2001). ECO was proposed to determine a network density threshold for filtering out the weakest links (De Vico Fallani, Latora, & Chavez, 2017). It maximizes an extension of J^{max}, the ratio between the overall (both global and local) efficiency and its wiring cost $\max_\rho J^{ext}(\rho) = (E_g(\rho) + E_{loc}(\rho))/\rho$, where E_{loc} denotes the network local efficiency. The study (Latora & Marchiori, 2001) also demonstrated that, to maximize J, these networks have to be sparse with an average node degree $K \simeq 3$.

Minimum spanning tree (MST). This is an increasingly popular method for identifying the smallest and most essential set of connections while ensuring that the network forms a fully

connected graph (Guo, Qin, Chen, Xu, & Xiang, 2017; Meier, Tewarie, & Van Mieghem, 2015; Otte et al., 2015; van Nieuwenhuizen et al., 2018). The tenet of using MST is to summarize information and index the structure of the graph, and thus remove edges with redundant information (Mantegna, 1999). Specifically, an MST filtered graph will contain N nodes connected via $N - 1$ connections with minimal cost and no loops. This addresses key issues in existing topology filtering schemes that rely on arbitrary and user-specified absolute thresholds or densities.

Orthogonal minimum spanning tree (OMST). This topological filtering scheme was proposed recently (S. Dimitriadis, Antonakakis, Simos, Fletcher, & Papanicolaou, 2017) to maximize the information flow over the network versus the cost by selecting the connections via the OMSTs. It samples the full-weighted brain network over consecutive rounds of MST that are orthogonal to each other. Practically, we extracted the first MST, and then we cleared their connections and we tracked the second MST from the rest of the network connections, and so forth. Such an iterative procedure (stopped by the Mth MST) can get orthogonal MSTs and topologically filter brain network by optimizing the GCE under the constrains by the MST, leading to an integration of both GCE and MST:

$$\max_{n \in [1,M]} J(\rho(n\text{MSTs})) = E_g(\rho(n\text{MSTs})) - \rho(n\text{MSTs})$$

Planar maximally filtered graph (PMFG). The idea underneath PMFG (Tumminello, Aste, Di Matteo, & Mantegna, 2005) is to filter a dense matrix of weights by retaining the largest possible subgraph while imposing global constraints on the derived network topology. Edges with the strong connection weights are retained while constraining the subgraph to be a (spanning) tree globally. Similarly, during the PMFG construction, the largest weights are retained while constraining the subgraph to be a planar graph globally. The PMFG algorithm searches for the maximum weighted planar subgraph by adding edges one by one. The resulting matrix is sparse with $3(N - 2)$ edges. It starts by sorting all the edges of a dense matrix of weights in nonincreasing order and tries to insert every edge in the PMFG. Edges that violate the planarity constraint are discarded.

Triangulated maximally filtered graph (TMFG). The algorithm for implementing PMFG is computationally expensive, and is therefore impractical when applied to large brain networks (Massara, Di Matteo, & Aste, 2016). A more efficient algorithm, TMFG, was developed that exhibited greatly reduced computational complexity compared to PMFG. This method captures the most relevant information between nodes by approximating the network connectivity matrix with the endorsement association matrix and minimizing spurious associations. The TMFG-derived network contains three-node (triangle) and four-node (tetrahedron) cliques, imposing a nested hierarchy and automatically generates a chordal network (Massara et al., 2016; Song, Di Matteo, & Aste, 2012). Although TMFG is not widely applied in network neuroscience studies, it has been applied elsewhere and proven to be a suitable choice for modeling interrelationships between psychological constructs like personality traits (Christensen, Kenett, Aste, Silvia, & Kwapil, 2018).

Orthogonal TMF graph (OTMFG). To combine both the TMFG's efficiency and OMST's accuracy, we propose OTMFG to maximize the information flow over the network versus the cost by selecting the connections of the orthogonal TMFG. It samples the full-weighted brain network over consecutive rounds of TMFG that are orthogonal to each other.

In summary, as illustrated in Figure 4A, the 12 edge filtering schemes transform a fully weighted matrix into a sparse matrix to represent the corresponding brain network. They can
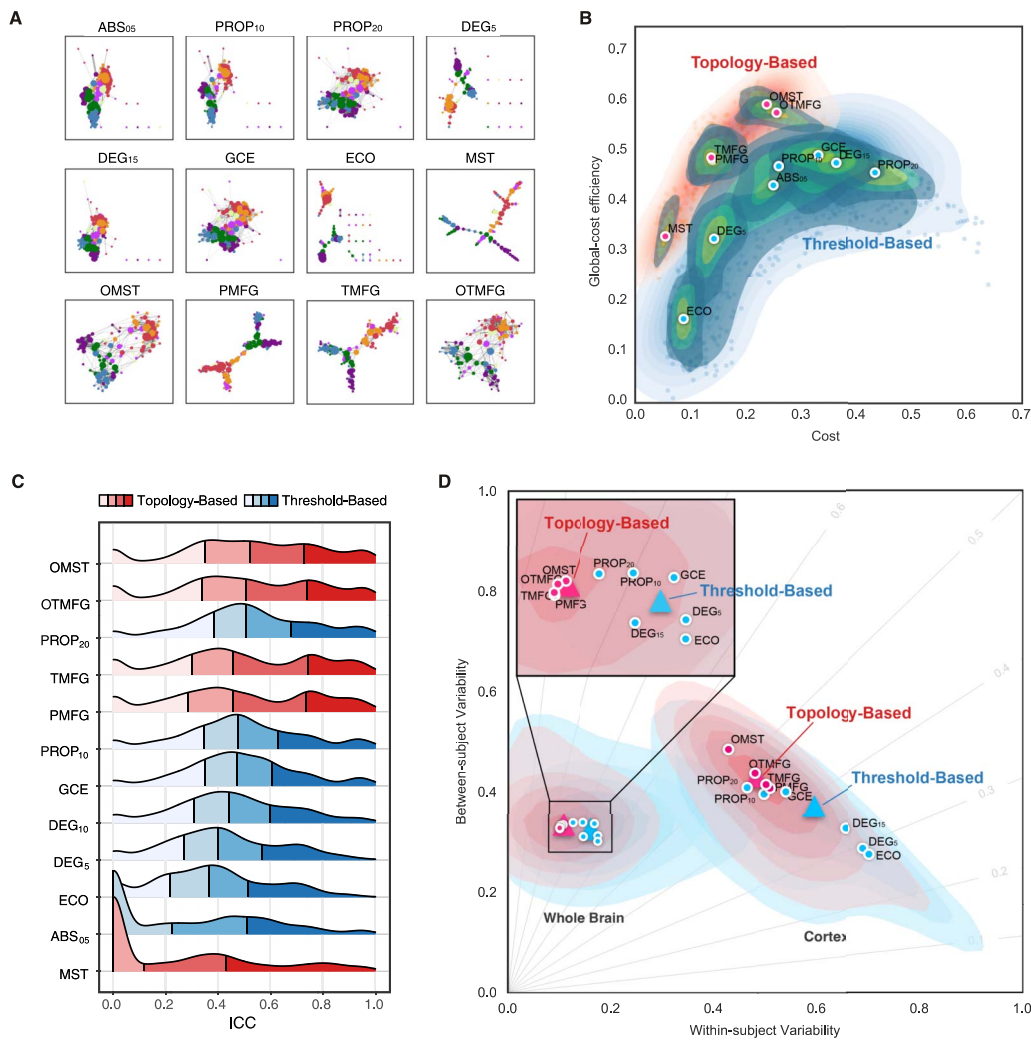
Figure 4. Edge filtering schemes and their networking performance. (A) Twelve schemes of filtering edge are applied to an individual connectivity matrix, resulting in the 12 brain networks with their nodes colored as the Yeo2011-7Networks (Thomas Yeo et al., 2011). (B) Global cost efficiency are plotted against network wiring costs of all the brain networks derived with the 12 edge filtering schemes from all the individual rfMRI scans. Red dots represent the topology-based, while blue dots are for threshold-based networks. These dot plots are fitted into the topographic (contour) maps where the local maxima for each filtering choice is labeled as a circle. (C) Density plots are for ICC distributions under various the 12 edge filtering schemes. These density distributions are ranked from top to bottom according to decreases of the mean ICCs, while the two colors depict the topology-based and threshold-based schemes. Four quartiles were indicated by vertical lines. (D) Network measurements are projected onto the reliability anatomy plane coordinated by both between- and within-subject variability. Red dots represent the topology-based, while blue dots are for threshold-based networks. The topographic (contour) maps fit the dots and label the local maxima as a circle for each scheme and the global maxima as a triangle for the topology and threshold groups, respectively.

be categorized into two classes: threshold-based versus topology-based schemes. ABS_{05}, $PROP_{10}$, $PROP_{20}$, DEG_5, DEG_{15}, ECO, and GCE rely on a threshold for filtering and retaining edges with higher weights than the threshold. These schemes normally ignore the topological structure of the entire network and can result in isolated nodes. In contrast, the topology-based methods including MST, OMST, PMFG, TMFG, and OTMFG all consider the global network topology in determining which edges to retain. As illustrated in Figure 4B, all the schemes are plotted in the $\rho - J^{max}$ plane for their network economics.

Table 1. A list of the employed network metrics derived with graph theory

	Measure	Attribute	Symbol	Reference
Global	Integration	Global efficiency of the network	Eg	Latora & Marchiori, 2001
		Average shortest path length of the network	Lp	Watts & Strogatz, 1998
		Pseudo diameter of the network	D	Bouttier, Di Francesco, & Guitter, 2003
	Segregation	Clustering coefficient of the network	Cp	Watts & Strogatz, 1998
		Local efficiency of the network	E_{local}	Latora & Marchiori, 2001
		Modularity of the network	Q	Newman, 2004
		Transitivity of the network	Tr	Newman, 2003
Nodal	Centrality	Local characteristic path length of nodes	Lp_i	Watts & Strogatz, 1998
		Efficiency of nodes	$E_{nodal,i}$	Latora & Marchiori, 2001
		Local efficiency of nodes	$E_{local,i}$	Latora & Marchiori, 2001
		Clustering coefficient of nodes	Cp_i	Watts & Strogatz, 1998
		Pagerank centrality of nodes	Pc_i	Page, Brin, Motwani, & Winograd, 1999
		Degree centrality of nodes	Dc_i	Pastor-Satorras, Vázquez, & Vespignani, 2001
		Eigenvector centrality of nodes	Ec_i	Newman, 2008
		Resolvent centrality of nodes	Rc_i	Estrada & Higham, 2010
		Subgraph centrality of nodes	Sc_i	Estrada & Rodriguez-Velazquez, 2005
		Betweenness centrality of nodes	Bc_i	Freeman, 1978

Network Analysis

We performed graph theory–driven network analysis by calculating several common graph-based metrics for the resulting graphs. These measures, broadly, can be interpreted based on whether they characterize the extent to which network structure allows for integrated or segregation information flow. Examples of integrative measures include average shortest path length (L_p), global efficiency (E_g), and pseudo diameter (D). Segregation measures include clustering coefficient (C_p), local efficiency (E_{local}), transitivity (Tr), modularity (Q), and a suite of nodal centrality measures (Table 1). All the metrics are calculated using the Brain Connectivity Toolbox (Rubinov & Sporns, 2010). We employed graph-tool (https://graph-tool.skewed.de) and NetworKit (https://networkit.github.io) to achieve high performance comparable (both in memory usage and computation time) to that of a pure C/C++ library.

RESULTS

Whole-brain Networks Are More Reliable Than Cortical Networks

We evaluated reliability based on 24 different parcellation choices (Figure 2A). In the following parts of the paper, we name a parcellation as '*ParcAbbr-NumberOfParcels*' (e.g., LGP-100 or its whole-brain version wbLGP-458). We found significant differences in ICC distributions across the 24 parcellation choices (Figure 2B, Friedman rank sum test: $\chi^2 = 20379.07$, $df = 23$,

$p < 2.2 \times 10^{-16}$, effect size $W_{Kendall} = 0.377$). The mean ICCs range from slight (LGP-1000) to substantial (wbLGP-458). Given a particular parcellation and definition of nodes, we illustrate the density distribution of its ICCs under all other strategies (edge definition and metric derivation). Notably, whole-brain parcellations yield higher measurement reliability than parcellations of cerebral cortex on their own (the effect sizes > 0.65). This improvement in reliability seems not simply a by-product of having more parcels. We chose the parcellations in which the number of parcels ($400 \leq n \leq 1,000$) almost overlapped between the cortex and the whole brain, and found no correlation between the number of parcels and the median ICCs ($r = -0.11$, $p = 0.7$). We report the mean ICC and the number of almost perfect (noap) ICCs (≥ 0.8) as the descriptive statistics for the density distributions. The wbLGP-458 (mean ICC: 0.671; noap ICC: 519), wbLGP-558 (mean ICC: 0.671; noap ICC: 540) and The wbBNP-568 (mean ICC: 0.664; noap ICC: 511) are the three most reliable choices (see more details of the post hoc Wilcoxon signed rank test in Supporting Information Table S7). Among the cortical parcellations, the LGP-500 (mean ICC: 0.362; noap ICC: 0), LGP-400 (mean ICC: 0.342; noap ICC: 0), and LGP-600 (mean ICC: 0.340; noap ICC: 0) are the three most reliable choices (Supporting Information Table S3).

To better understand the effect of introducing 358 subcortical parcels into the cortical parcellations, we decomposed the reliability changes into a two-dimensional representation of changes of individual variability (Figure 2C, and D). This idea was motivated by the analysis of reliability derived with individual variability (Xing & Zuo, 2018; Zuo, Xu, & Milham, 2019b) as in Figure 1C. For each ICC under a given parcellation choice, we calculated the related between-subject variability V_b and within-subject variability V_w. Changes in the individual variability associated with the reliability improvements from cortical to whole-brain pipelines were plotted along with ΔV_b and ΔV_w as arrows. These arrows are distributed across the three quadrants (quadI: 0.94%; quadII: 59.99%; quadIII: 39.07%). We noticed that most of these arrows were distributed into the optimal quadrant where the improvements of test-retest reliability by the whole-brain parcellation choices largely attributing to the increases of between-subject variability and decreases of within-subject variability. The decreases of both between-subject and within-subject variability may also strengthen the measurement reliability (the suboptimal quadIII in Figure 2).

Spontaneous brain acitivity:
Activity not attributable to specific brain inputs or outputs and representative neuronal activity intrinsically generated and organized in the brain.

Spontaneous Brain Activity Portrays More Reliable Networks in Higher Slow Bands

Brain oscillations are hierarchically organized, and their frequency bands were theoretically driven by the natural logarithm linear law (Buzsaki & Draguhn, 2004). By analogy, rfMRI oscillations can, similarly, be partitioned into distinct frequency bands. Advanced by the fast imaging protocols (TR = 720 ms), HCP test-retest data allow to obtain more oscillation classes than traditional rfMRI acquisitions (typical TR = 2 s). We incorporate Buzsaki's framework with the HCP dataset using the DREAM toolbox (Gong et al., 2021) in the Connectome Computation System to decompose the time series into the six slow bands (Figure 3A): slow-6 (0.0069–0.0116 Hz), slow-5 (0.0116–0.0301 Hz), slow-4 (0.0301–0.0822 Hz), slow-3 (0.0822–0.2234 Hz), slow-2 (0.2234–0.6065 Hz), and slow-1⁻ (0.6065–0.6944 Hz).

We noticed that, due to the limited sampling rate (TR), this slow-1⁻ only covers a small part of the full slow-1 band (0.6065–1.6487 Hz) – we indicate this above. We also included the frequency band, slow-emp (0.01–0.08 Hz) for the sake of comparison, as it is covers a range commonly used in rfMRI studies. A significant effect on order ($\chi^2 = 9283.536$, $df = 6$, $p < 2.2 \times 10^{-16}$, $W_{Kendall} = 0.192$) across the frequency bands was revealed based on the density distributions of ICC (Figure 3B): slow-2, slow-1⁻, slow-3, slow-emp, slow-4, slow-5, and slow-6.

Post hoc paired tests indicated that any pairs of neighboring bands are significantly different from one another, with measurement reliability increasing with faster frequency bands. Note, however, that slow-1$^-$ (mean ICC: 0.564) did not fit into this trend, possibly due to its limited coverage of the full band. But remarkably, slow-1$^-$ exhibited the largest number of almost pre-fect ICCs for potential reliability (noap ICC: 1746). Slow-emp (mean ICC: 0.519; noap ICC: 434) contains overlapping frequencies with both slow-4 (mean ICC: 0.560; noap ICC: 441) and slow-5 (mean ICC: 0.494; noap ICC: 285), and higher ICCs than the two bands but the effect sizes are small to moderate (slow-emp vs. slow-4: 0.193; slow-emp vs. slow-5: 0.485). Slow-6 is the choice with the lowest ICCs (mean ICC: 0.331; noap ICC: 154) compared to other bands (large effect sizes: $r > 0.57$).

To visualize reliability variation across frequency bands, we plotted a trajectory tracing reliability flow along the five full (slow-6 to slow-2) bands in the reliability plane, whose axes correspond to between-versus within-subject variability (Figure 3C). As expected, this nonlinear trajectory contains two stages of almost linear changes of the network measurement reliability from slow to fast oscillations: whole brain versus cortex. In each case, the reliability improvements attribute to both increases of between-subject variability and decreases of within-subject variability while the improvements of whole-brain network measurement reliability were largely driven by the increased variability between subjects.

Topological Economics Individualize Highly Reliable Functional Brain Networks

Estimating functional connections can be highly challenging due to the absence of a 'ground truth' human functional connectome. To provide a reliable way of building candidate edges of the connections, we sampled the 12 schemes on graph edge filtering (Figure 4A), which turn a fully connected matrix into a sparse graphical representation of the corresponding brain network. These schemes can be categorized into two classes: threshold-based versus topology-based schemes. Threshold-based schemes usually use a threshold to preserve those edges whose strengths are above a cutoff value, such as ABS_{05}, $PROP_{10}$, $PROP_{20}$, DEG_5, and DEG_{15}. Threshold-based schemes are widely used in network neuroscience and ignore the intrinsic topological structure of the entire brain network (e.g., leading to multiple connected components or isolated nodes). In contrast, topology-based schemes such as MST, OMST, PMFG and TMFG come from other scientific disciplines and are optimized based on the entire network topology (see Materials and Methods). To combine both the TMFG's efficiency and OMST's accuracy, we proposed the OTMFG. All the schemes are plotted in the plane of cost versus global cost efficiency to better visualize the economical properties of the derived networks (Figure 4B). These plots are fitted into the topographic (contour) maps where the local maxima for each filtering choice is labeled as a circle. The human brain networks achieve higher global efficiency with lower cost by using topology-based schemes compared to threshold-based schemes, suggesting increasingly optimal economics.

Significant differences in test-retest reliability were detectable across these 12 edge filtering schemes ($\chi^2 = 9784.317$, $df = 11$, $p < 2.2 \times 10^{-16}$, $W_{Kendall} = 0.189$, see Figure 4C). Among the topology-based schemes, OMST (mean ICC: 0.608; noap ICC: 765), OTMFG (mean ICC: 0.602; noap ICC: 781), and TMFG (mean ICC: 0.570; noap ICC: 767) were the three most reliable choices. They showed significantly greater reliability than the three most reliable threshold-based, respectively: $PROP_{20}$ (mean ICC: 0.593; noap ICC: 632), $PROP_{10}$ (mean ICC: 549; noap ICC: 445), and GCE (mean ICC: 0.533; noap ICC: 352). Mean reliability of MST are slight to fair (mean ICC: 0.309) but its number of almost perfect reliability (noap ICC:362) is still higher than all threshold-based schemes except $PROP_{10}$ and $PROP_{20}$.

Network measurements are labeled based on topology and threshold groups and projected onto the reliability anatomy plane, whose axes represent between- and within-subject variability (Figure 4D). The contour maps are reconstructed for each scheme based upon the individual variability of all the related network measurements. The topology-based methods (red) showed overall higher ICCs than the threshold-based methods (blue), improvements that could be attributed to increases in between-subject variability and decreases of within-subject variability. These observations are consistent between cortex and whole-brain networks while topology-based whole brain network are almost perfectly reliable (meaning almost perfect reliability, i.e., ICC ≥ 0.8).

We also explored connection transformation and edge weights, two factors included in edge filtering, the choices of connectivity transformation, and weighing edges, regarding their measurement reliability. Positive (Equation pos) (mean ICC: 0.512; noap ICC: 1,031) and exponential (Equation exp) transformation (mean ICC: 0.509; noap ICC: 1,855) were the two most reliable choices. Comparing to the positive and absolute (Equation abs) transformation (mean ICC: 0.508; noap ICC: 1,050) transformation, the exponential and distance-inverse (Equation div) (mean ICC: 0.500; noap ICC: 1,031) transformation show larger number of almost perfect ICCs. Weighted graphs are also more reliable than the binary graphs, while the normalized weighted graphs demonstrated the highest ICCs, reflecting both the increased between-subject variability and decreased within-subject variability.

Network Integration and Segregation Can Serve Reliable Metrics of Information Flow

The previous extensive data analysis suggests that the optimally reliable pipeline should (1) define network nodes using a whole-brain parcellation, (2) filter the time series with higher frequency bands, (3) transform the connectivity using positive transformation, and (4) construct network edges using topology-based methods and normalized weights. Using the optimal pipelines, we evaluated the reliability levels of various metrics from network neuroscience and their differences across individuals. Focusing on the optimized pipeline with the highest ICCs of the various choices (wbLGP-458, slow-2, pos, normalized weights, OMST), we reported test-retest reliability of the measurements as well as their corresponding individual variability. In Figure 5A, we found that the global network measurements of information segregation and integration are at the level of almost perfect reliability except for the modularity Q (ICC = 0.46, 95% CI = [0.252, 0.625]). These high-level ICCs are derived with large between-subject variability and small within-subject variability (Figure 5B). These findings are reproducible across the other two parcellation choices (wbCABP-718, wbBNP-458). In consideration of "Ease-of-Use" for researchers and higher cortical resolution, we mapped the "Out-of-the-Box" Cole-Anticevic Brain-wide Network Partition (wbCABP-718) for nodal metrics visualization.

Similar to the global metrics, shortest path length L_p and nodal efficiency E_{nodal} exhibited the highest ICCs (almost perfect test-retest reliability), while ICCs of other nodal metrics remained less than 0.6. To visualize node-level network metrics, we reported results derived from the wbCABP-718 choice. To improve spatial contrasts of reliability, we ranked the parcels according to their ICCs and visualized the ranks in Figure 5C. Most nodal metrics are more reliable across the 360 cortical areas than the 358 subcortical areas (Wilcoxon tests: all p values less than 0.001, corrected for multiple comparisons). However, L_p, E_{nodal}, and B_c exhibited higher across subcortical areas than cortical areas (corrected $p < 0.001$). Across the human cerebral cortex, the right hemispheric areas demonstrated more reliable C_p (corrected $p < 0.0036$) than the left hemispheric areas. Interesting patterns of the reliability gradient are also
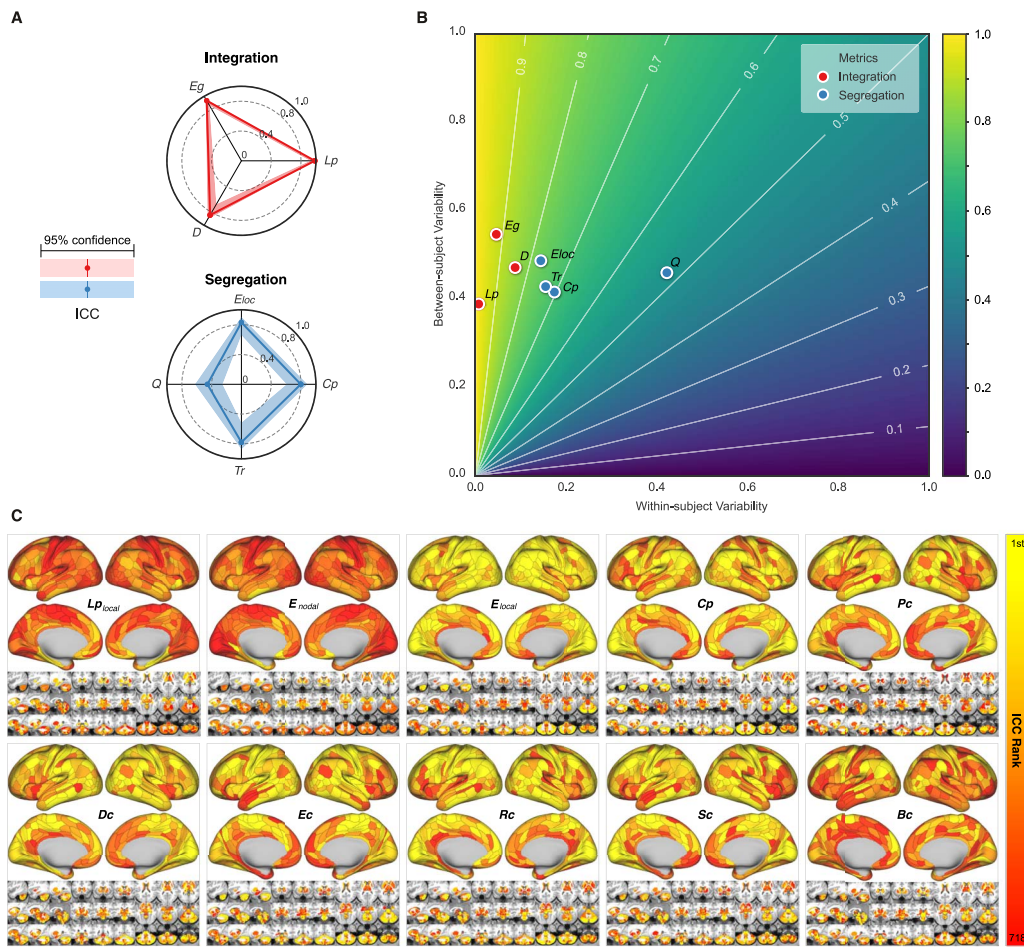
Figure 5. Measurement reliability and variability of global/nodal network metrics under the optimized pipeline. (A) Spider plots are visualized for ICCs (test-retest) with the 95% confidence intervals (CIs, shadow bands) for the global metrics of network integration, segregation. Integrative measures include average shortest path length (L_p), global efficiency (E_g), and pseudo diameter (D). Segregation measures include clustering coefficient (C_p), local efficiency (E_{loc}), transitivity (Tr), and modularity (Q). (B) The reliability anatomy was plotted as a function of between-subject variability (V_b) and within-subject variability (V_w). (C) Ranks of ICCs across the 360 cortical parcels and the 358 subcortical parcels in the optimal pipeline (wbCABP-718, slow-2, pos, OMST) are depicted. Ten nodal metrics are assessed including local characteristic path length of node (Lp_{local}), nodal efficiency (E_{nodal}), local efficiency of nodes (E_{local}), nodal clustering coefficient (C_p), pagerank centrality (P_c), degree centrality (D_c), eigenvector centrality (E_c), resolvent centrality (R_c), subgraph centrality (S_c), and betweeness centrality (B_c).

observable along large-scale anatomical directions (dorsal > ventral, posterior > anterior) across the nodal metrics of information segregation and centrality. These spatial configuration profiles on the reliability reflected their correspondence on interindividual variability of these metrics, characterising the network information flow through the slow-2 band.

Building An Open Resource for Reliable Network Neuroscience

The results presented here represent huge costs in terms of computational resources (more than 1,728,000 core-hours on CNGrid), supported by Chinese Academy of Sciences (https://cscgrid .cas.cn). Derivations of the ICCs and their linear mixed models were implemented in R and Python. As is our practice in open science, we have started to provide an online platform on the reliability assessments (https://ibraindata.com/research/ifNN/reliabilityassessment). The big reliability data were designed into an online database for providing the community a resource to search reliable choices and help with final decision-making. The website for this

online database provided more details of the reliability data use. We shared all the codes, figures, and other reliability resources via the website (https://ibraindata.com/research/ifNN /database).

DISCUSSION

This study examined the series of processing and analysis decisions in constructing graphical representations of brains' intrinsic spontaneous activity. The focus, here, was on identifying the pipeline that generated reliable, individualized networks and network metrics. The results of our study suggest that to derive reliable global network metrics showing higher interindividual variances and lower intraindividual variances, one should use whole-brain parcellations to define network nodes, focus on higher frequencies in the slow band for time series filtering to derive the connectivity, and use the topology-based methods for edge filtering to construct sparse brain graphs. Regarding network metrics, multilevel or multimodal metrics appear more reliable than single-level or single-model metrics. Deriving reliable measurements is critical in network neuroscience, especially for translating network neuroscience into personalized practice. Based on these results, we provide four principles toward optimal functional network neuroscience for reliability of measuring individual differences.

Principle I: Use A Whole Brain Parcellation to Define Network Nodes

The basic unit of a graph is the node. However, variability across brain parcellations can yield different graphs, distorting network metrics and making it difficult to compare findings across studies (Wang et al., 2009; Zalesky et al., 2010). In many clinical applications (Fornito et al., 2015; Matthews & Hampshire, 2016) researchers aim to identify disease-specific connectivity profiles of the whole brain, including cortical and subcortical structures, as well as cerebellum. A recent review has raised the concern that many studies have focused on restricted sets of nodes, for example, cortex only, and has called for a field standard for the best practices in clinical network neuroscience (Hallquist & Hillary, 2019), which requires almost perfectly reliable measurements (Xing & Zuo, 2018). Our meta-reliability assessments revealed such high reliability of measurements made involving functional brain networks can be achieved, through the inclusion of high-resolution subcortical nodes. This provides strong evidence that whole-brain node use should be part of the standard analysis pipeline for network neuroscience applications. These improvements of reliability can be attributed to increases in between-subject variability coupled with reductions in within-subject variability relative to networks of cortical regions alone. One possible neuroanatomical explanation is that distant areas of cerebral cortex are interconnected by the basal ganglia and thalamus while also communicating with different regions of the cerebellum via polysynaptic circuits, forming an integrated connectome (Bostan & Strick, 2018). These subcortical structures have been suggested to play a role in both primary (e.g., motor) and higher order function (e.g., learning and memory), while studies using rfMRI have delineated the resting-state functional connectivity (RSFC) maps between these subcortical structures and cortical networks of both primary and high-order functions. Interestingly, a recent work revealed that interindividual variance in cerebellar RSFC networks exceeds that of cortex (Marek et al., 2018). Meanwhile, these RSFC maps are highly individualized and stable within individuals (D. Greene et al., 2020), indicating that they possess reliable characteristics. In line with our observations, we argue that inclusion of the subcortical structures as network nodes can enhance the between-subject variability and stabilize the within-subject variability by providing more comprehensive measurements on the entirety of the brain connectivity.

Principle II: Generate Functional Networks using Spontaneous Brain Activity in Multiple Slow Bands

It has been a common practice in rfMRI research to estimate the RSFC profile based on BOLD time series of the intrinsic spontaneous brain activity from the low frequency (0.01–0.1 Hz or 0.01–0.08 Hz). However, the test-retest reliability of RSFC measurements derived from this frequency band has been limited, with ICCs less than 0.4 (Noble et al., 2019; Zuo & Xing, 2014). Existing studies, however, have advocated adopting a multifrequency perspective to examine the amplitude of brain activity at rest (Zuo et al., 2010) and its network properties (Achard et al., 2006). This approach has been spurred along by recent advances in multi-banded acquisitions and fast imaging protocols, offering rfMRI studies a way to examine spontaneous brain activity at much higher frequencies that may contain neurobiologically meaningful signals (Gong et al., 2021). Our study provides strong evidence of highly reliable signals across higher slow-frequency bands, which are derived with the hierarchical frequency band theory of neuronal oscillation system (Buzsaki & Draguhn, 2004). Specifically, a spectrum of reliability increases was evident from slow bands to fast bands. This reflects greater variability of the network measurements between subjects and less measurement variability within subject between the higher and lower bands of the slow frequencies. In theory, each frequency band has an independent role in supporting brain function. Lower frequency bands are thought to support more general or global computation with long-distance connections to integrate specific or local computation, which are driven by higher slow bands based on short-distance connections (Buzsáki, 2009). Our findings of high reliability (interindividual differences) are perfectly consistent with this theory from a perspective of individual variability. Previous findings have found that high-order associative (e.g., default mode and cognitive control) networks are more reliable than the primary (e.g., somatomotor and visual) networks (Noble et al., 2019; Zuo & Xing, 2014; Zuo, Xu, & Milham, 2019b). A novel frequency-based perspective on these network-level individual differences can be inspired directly by our observations on the multiple bands.

Principle III: Optimize Topological Economy to Construct Network Connections at Individual Level

There is no gold standard on for human functional connectomes, leading to a plurality of approaches for inferring and constructing brain network connections. Threshold-based methods focus on the absolute strength of connectivity, retaining connections that are above some user-defined threshold and oftentimes involve applying the same threshold to all subjects. Although this approach mitigates potential biases in network metrics associated with differences in network density, it may inadvertently also lead to decreased variability between subjects. This is supported by our results showing that threshold-based methods yield low reliability of network measurements. On the other hand, the human brain is a complex network that is also near optimal in terms of connectional economy, balancing trade-offs of cost with functionality (Bullmore & Sporns, 2012). In line with this view, certain classes of topology-based methods for connection definition may hold promise for individualized network construction. Specifically, each individual brain optimizes its economic wiring in terms of cost and efficiency, reaching a trade-off between minimizing costs and allowing the emergence of adaptive topology. Our results demonstrate that such highly individualized functional connectomes generated by the topology-based methods are more reliable than those generated by the threshold-methods. This reflects the increase of individual differences in functional connectomes attributing to the optimal wiring economics at individual level. The topological optimization also brings other benefits such as ensuring that a graph forms a single connected component and preserving weak connections. Indeed, there is increasing evidence supporting the hypothesis that weak connections are neurobiologically meaningful and explain individual

differences in mind, behavior, and demographics as well as disorders (Santarnecchi, Galli, Polizzotto, Rossi, & Rossi, 2014). Weak connections in a graph may be consistent across datasets and reproducible within the same individual over multiple scanning sessions and therefore be reliable. Weak connections might also play nontrivial roles in transformed versions of the original brain network, for example, so-called "edge-based functional connectivity" (Faskowitz, Esfahlani, Jo, Sporns, & Betzel, 2020). Among these topology-based methods, MST is the simplest and most promising filtering method if computational efficiency is the priority. MST can obtain a graph with the same number of nodes and edges, and it is not sensitive to scaling effects, because its structure only depends on the order rather than the absolute values of the edges. Although MST loses some local network measurements due to the limited number of edges, it has some other unique metrics that can be calculated (e.g., leaf fraction, tree hierarchy). A better alternative might be TMFG, which is computationally very efficient and statistically robust, while the OMST and OTMFG are the most reliable choices by prioritizing significant individual differences.

Principle IV: Characterize Information Flow with Both Network Integration and Segregation Metrics

Intrinsic functional networks reflect the outcomes of communication processes and information flows between pairs of brain regions. How the information and other signals propagate between pairs of brain regions can be assayed using network neuroscientific metrics and is essential to understanding normative connectome function and its variation in clinical settings. While the ground truth of functional connectome remains unknown (and may not exist), network models can help validate the imaging-based reconstructions of human functional networks (D. Bassett et al., 2020). From a perspective of individual differences, reliable network measures are the basis of achieving valid ifNN measurements (Zuo, Xu, & Milham, 2019b). Our findings indicated that both the brain network segregation and integration could be reliably measured with functional connectomics using rfMRI by the optimized pipelines. At the global level, measures of information integration, for example, characteristic path length and efficiency, were more reliable than those of information segregation, for example, modularity and clustering coefficient. Our results also revealed that measures of integration were more stable across different scan sessions (i.e., the test-retest) for an individual subject than the segregation measurements, while interindividual variability are measured at the similar level for both integration and segregation metrics. At the nodal level, mapping reliability of the network measurements revealed interesting spatial patterns. Specifically, we found that cortical areas were generally associated with more reliable local measurements compared to subcortical areas. This may reflect different functional roles for human cortex and subcortex. For example, the differences in reliability of path-based metrics might reflect the fact that there are more cortical within-community paths, while between-community paths are more common in subcortex. Beyond this cortical-subcortical gradient, reliability of the nodal information flow also fit the left-right asymmetry and dorsal-ventral as well as posterior-anterior gradient, implying the potential validity of individual differences in information flow attributing to evolutionary, genetic, and anatomical factors (Chen et al., 2013; Rakic, 2009). To facilitate the utility of reliable network integration and segregation metrics in ifNN, we integrated all the reliability resources into an online platform for reliability queries on specific metrics of information flow (https://ibraindata.com/research/ifNN).

Reproducibility and Generalizability

Both reproducibility and generalizability are cornerstones of modern sciences, and remain challenging as a scientific research frontier (Munafo et al., 2017; Yarkoni, 2022). In this

research, we adopt a big data approach by deeply sampling the parameters (more than 524k parametric settings) of various steps in the network construction and analysis pipeline to systematically explore the reliability of functional brain network measurements. This provided robust experimental evidence supporting four key principles that will foster optimal ifNN research and application. These principles can serve as the basis for building guidelines on the use of ifNN to map individual differences. Standard guidelines are essential for improvements of reproducibility and generalizability in research practice, and our work provides basic resources, initiating such standardization in future network neuroscience. We note, however, that while our approach was extensive, it was not exhaustive (likely impossible)—the analytical sampling procedure could miss many other existing choices. The processing decisions that yield reliable connectomic measurements may yield the most reliable network statistics, but there may be another way to process data that yields overall a higher level of reliability in network measures. Regarding the statistical benefits of our sampling analytics in the parametric space of the ifNN pipelines, we discuss below the implications of the present research for reproducible and generalizable network neuroscience.

Reliability and validity. Pipelines of generating highly reliable measurements are central to the experimental design of studying individual differences (Matheson, 2019; Zuo, Xu, & Milham, 2019b). Given a statistical power, for a fixed sample size, experiments designed with more reliable pipelines can detect bigger effects of interests. On the other side, to detect a fixed effect size, experiments designed with more reliable pipelines would be more powerful or logistically economical (e.g., needless samples). This has very important implications on the recent arguments about "big data versus small data" (Marek et al., 2022; Rosenberg & Finn, 2022; Tibon, Geerligs, & Campbell, 2022), which must take the reliability into account when first designing an experiment (Gratton, Nelson, & Gordon, 2022), and has been increasingly appreciated by the field of network neuroscience (Helwegen, Libedinsky, & van den Heuvel, 2023). From a perspective of experimental design, reliability is more straightforward to reproducibility but validity is related to generalizability. Therefore, we clarify that the measurement reliability is not the final goal but the validity (Finn & Rosenberg, 2021; Noble et al., 2021), which is not easily ready for a direct examination as a reliability assessment (Zuo, Xu, & Milham, 2019b). The reliable pipeline we proposed produced biologically plausible findings according to the four principles we discussed, likely reflecting its potential validity of measuring individual differences in intrinsic brain functional organization. Validation on the use of our proposed principles represents a promising arena for fostering future network neuroscience studies such as personality (Hilger & Markett, 2021) or brain developmental charts (Bethlehem et al., 2022), with potential novel fMRI paradigms (Elliott, Knodt, & Hariri, 2021b; Finn, Glerean, Hasson, & Vanderwal, 2022) or more precise neuroimaging technology (Toi et al., 2022).

Reliability does not necessarily equate to but indeed provides an up bound of validity. In some cases, increasing reliability may cause a decrease in validity, particularly if the sources of reliability are not related to the underlying construct of interests. For example, physiological noise and head motion can be highly reliable as biological traits, but may not be involved in the investigated cognitive processes. Previous studies have shown that head motion can introduce artifacts into the fMRI data, which can affect the reliability of functional connectivity measures (Power et al., 2014). In particular, head motion may have a nonuniform impact on different edge filtering methods and network metrics. Certain methods that rely on the strength of functional connections, such as threshold-based approaches, may be more sensitive to head motion artifacts than topology-based methods that focus on the overall structure of the network. Measures that are highly reliable due to the inclusion of these contaminants may

not be valid indicators of the underlying construct. However, head motion may not always be purely noise and may contain some neurobiologically meaningful signals (Zeng et al., 2014; Zhou et al., 2016). Therefore, it is important to carefully consider the potential impact of head motion when choosing an edge filtering method and interpreting the resulting functional connectivity measures, as well as the trade-off between controlling for motion artifacts and preserving potentially meaningful signals in the data. In the context of graph theory, noise can affect both the reliability and validity of graph metrics. For example, noise in the data can result in higher reliability of certain graph metrics, but this may not necessarily reflect the true underlying network structure. This is because noise may lead to inflated correlations between certain regions, resulting in overestimations of network connectivity and thus higher reliability. However, these measurements may not be valid indicators of the true network structure and may not accurately reflect the underlying cognitive processes being studied. On the other hand, the removal of noise may lead to decreased reliability, but may improve the validity of the measurement by reducing the influence of unrelated sources of variance. The optimal choices for maximizing reliability in our study may also have implications for interpretability and generalizability. For example, the inclusion of subcortical structures in the parcellation scheme may increase the interpretability of the results, as these structures play a key role in the functional organization of the brain. On the other hand, the choice of connectivity transformation and edge weighting may have implications for the generalizability of the results, as different methods may produce different results depending on the specific characteristics of the data. Further research is warranted to fully understand the consequences of these choices on interpretability, generalizability, and other aspects of the measurement process.

The rfMRI datasets minimally preprocessed by the HCP pipeline are employed for our study while many different pipelines are available for rfMRI data preprocessing (see a list of pipelines in Xu et al., 2015). These different pipelines vary across parametric settings and orders of various steps of preprocessing, and thus can have different impacts on the reliability of measuring spontaneous brain activity (Li et al., 2022). Therefore, it is very important to validate whether the present findings are reproducible under another preprocessing pipeline. Accordingly, we repeated our analyses by leveraging another widely accepted preprocessing pipeline, fMRIPrep (Esteban et al., 2019). As documented in the Supporting Information, the major findings supporting the principal guidelines are reproducible while the measurement reliability derived with fMRIPrep are generally lower than those with the HCP pipeline. Various within-pipeline parametric settings also as exist other choices not sampled by our experimental design but remain potentials for further investigation. For example, edge filtering methods are commonly used for identification and retain only the most important edges in a graph, based on criteria such as statistical significance or functional relevance. However, this approach has the potential to introduce bias and subjectivity in the selection process, and may not fully capture the higher order structure of a network system. Algebraic topology, as demonstrated by Giusti, Ghrist, and Bassett (2016) and other recent studies, offers a promising alternative for high-order edge filtering. By representing relationships between objects as higher dimensional simplices instead of edges, simplicial complexes can characterize polyadic interactions and capture more nuanced aspects of complex network organization. With the increasing availability of computational tools for the application of algebraic topology to real data, this framework has the potential to surpass graph theory in understanding the complexities of neural systems.

Other fMRI paradigms.   The guidelines we proposed for rfMRI-based network neuroscience may also provide insights for network neuroscience computation by leveraging task-fMRI or

movie-fMRI. These two paradigms have gained increasing attention in recent years as a means of measuring functional connectomes (Cole, Bassett, Power, Braver, & Petersen, 2014; Cole et al., 2013; Finn et al., 2022). The reliability and predictive power of these measures have been the subject of a number of studies. For instance, a study by Gao et al. (2020) found that the reliability of movie-fMRI connectivity was influenced by the complexity and duration of the movie stimulus, with more complex and longer stimuli resulting in higher test-retest reliability. A recent work demonstrated that these improvements of prediction with task-based functional connectivity were due largely to specific task design, highlighting the importance of task design in probing valid brain–behavior associations (Zhao et al., 2023). Such task-based fMRI connectivity methods can detect developmentally related individual differences in brain and behavior (Kardan et al., 2022). These findings support the notion that task-fMRI and movie-fMRI can produce more reliable connectivity measures with greater predictive power for individual differences in cognitive and mental health measures compared to rfMRI, particularly for tasks and stimuli that elicit strong and sustained activation. According to the relationships among rest, task, and movie as well as other naturalistic states of the human brain as a systems entity (Cole, Ito, Bassett, & Schultz, 2016; Finn, 2021; McCormick, Arnemann, Ito, Hanson, & Cole, 2022), we speculate that the four principles are generalizable to functional network neuroscience based on these nonrest brain states. However, we note that more research is warranted to fully understand the underlying mechanisms and generalizability of these findings to different task and movie paradigms as well as their translational applications (Eickhoff, Milham, & Vanderwal, 2020; Finn & Rosenberg, 2021).

Psychometric and other limitations.   When studying the individual differences in brain and behavior, one must consider the specific research aims and the underlying assumptions of the study for addressing the reliability trade-off between maximizing between-individual variability and minimizing within-individual variability. For example, if the goal of the study is to identify population-level age-related trajectories, it may be more important to prioritize maximizing between-individual variability in order to capture the full range of individual differences for a specific population. On the other hand, if the focus of the study is on assessing within-subject changes over time (e.g., the individual-level growth), it may be more important to minimize within-individual variance in order to accurately capture developmental changes in brain function. It is also important to consider the potential impacts of these trade-off decisions on the validity of measurements of interest. For example, if motion scrubbing or outlier detection leads to the exclusion of a large number of subjects or time points, this may introduce bias and reduce the generalizability of the results regarding the limited population diversity or temporal stability. Careful consideration of these trade-offs is therefore essential in order to ensure that the chosen approach is appropriate for the specific research aims and assumptions of the study. The reliability theory we proposed leads to a quantitative framework on the measurement reliability, which delineates the anatomy of reliability changes as a function of variability changes for both between and within individuals. Our demonstration of the utility of this framework as a compass of variability (see Figure 2C) can guide the decision-making in the experimental design as mentioned above.

The design of a psychometric study is normally recommended to recruit a group of participants who are stable across the duration of investigation. The stability makes the interpretation of within-subject variability straightforward as the subject-independent random noise, and the reliability assessment are more precise; this is also why most psychometric studies were done in adults although some in children (but with very short duration). Population diversity plays a critical factor of assuring the generalizability in studying individual differences (A. S. Greene et al., 2022; Ricard et al., 2023). This has been responded by the emerging population

neuroscience as a new stage of cognitive neuroscience to increase generalizability across populations. (Falk et al., 2013; Paus, 2010). Psychometric studies are particularly required for population neuroscience due to the core aim of measuring individual differences in brain and mind developmental during the life-span (Zuo et al., 2017, 2018). Future psychometric studies on network neuroscience including those further validating the four principles developed by the present work should be done for more diverse populations.

Summary and Conclusion

In this study we developed a novel framework to model reliability changes as a function of changes of between-subject and within-subject variability. This framework was leveraged to optimize network neuroscience computation of individual differences in human spontaneous brain activity for test-retest reliability. We showed that reliable network neuroscience computation should define network nodes with whole-brain parcellations, derive the network edge weights with spontaneous high-frequency slow-band oscillations, and construct the brain networks using topology-based methods for multilevel and multimodal characteristics. Our findings highlight the importance of psychometric studies to understand the individual differences in spontaneous brain activity at systems level, and provide the resources and principles of experimental design to guide future network neuroscience studies.

SUPPORTING INFORMATION

Supporting information for this article is available at https://doi.org/10.1162/netn_a_00315.

AUTHOR CONTRIBUTIONS

Chao Jiang: Conceptualization; Data curation; Formal analysis; Methodology; Resources; Software; Visualization; Writing—Original draft; Writing—Review & editing. Ye He: Conceptualization; Writing—Review & editing. Richard F. Betzel: Funding acquisition; Writing—Original draft; Writing—Review & editing. Yin-Shan Wang: Conceptualization; Writing—Review & editing. Xiu-Xia Xing: Conceptualization; Resources; Software; Supervision; Writing—Review & editing. Xi-Nian Zuo: Conceptualization; Data curation; Formal analysis; Funding acquisition; Investigation; Methodology; Project administration; Resources; Software; Supervision; Validation; Visualization; Writing—Original draft; Writing—Review & editing.

REFERENCES

Achard, S., Salvador, R., Whitcher, B., Suckling, J., & Bullmore, E. (2006). A resilient, low-frequency, small-world human brain functional network with highly connected association cortical hubs. *Journal of Neuroscience*, 26(1), 63–72. https://doi.org/10.1523/JNEUROSCI.3874-05.2006, PubMed: 16399673

Aurich, N., Filho, J., da Silva, A., & Franco, A. (2015). Evaluating the reliability of different preprocessing steps to estimate graph theoretical measures in resting state fMRI data. *Frontiers in Neuroscience*, 9, 48. https://doi.org/10.3389/fnins.2015.00048, PubMed: 25745384

Bassett, D., Bullmore, E., Meyer-Lindenberg, A., Apud, J., Weinberger, D., & Coppola, R. (2009). Cognitive fitness of cost-efficient brain functional networks. *Proceedings of the National Academy of Sciences*, 106(28), 11747–11752. https://doi.org/10.1073/pnas.0903641106, PubMed: 19564605

Bassett, D., Cullen, K., Eickhoff, S., Farah, M., Goda, Y., Haggard, P., ... Ueda, H. (2020). Reflections on the past two decades of neuroscience. *Nature Reviews Neuroscience*, 21(10), 524–534. https://doi.org/10.1038/s41583-020-0363-6, PubMed: 32879507

Bassett, D. S., Bullmore, E., Verchinski, B. A., Mattay, V. S., Weinberger, D. R., & Meyer-Lindenberg, A. (2008). Hierarchical organization of human cortical networks in health and schizophrenia. *Journal of Neuroscience*, 28(37), 9239–9248. https://doi.org/10.1523/JNEUROSCI.1929-08.2008, PubMed: 18784304

Bethlehem, R., Seidlitz, J., White, S., Vogel, J., Anderson, K., Adamson, C., ... Alexander-Bloch, A. F. (2022). Brain charts for the human lifespan. *Nature*, 604(7906), 525–533. https://doi.org/10.1038/s41586-022-04554-y, PubMed: 35388223

Biswal, B., Mennes, M., Zuo, X.-N., Gohel, S., Kelly, C., Smith, S., ... Milham, M. (2010). Toward discovery science of human brain function. *Proceedings of the National Academy of Sciences*, 107(10), 4734–4739. https://doi.org/10.1073/pnas.0911855107, PubMed: 20176931

Biswal, B., Zerrin Yetkin, F., Haughton, V., & Hyde, J. (1995). Functional connectivity in the motor cortex of resting human brain using echo-planar MRI. *Magnetic Resonance in Medicine*, 34(4), 537–541. https://doi.org/10.1002/mrm.1910340409, PubMed: 8524021

Bostan, A., & Strick, P. (2018). The basal ganglia and the cerebellum: Nodes in an integrated network. *Nature Reviews Neuroscience*, 19(6), 338–350. https://doi.org/10.1038/s41583-018-0002-7, PubMed: 29643480

Botvinik-Nezer, R., Holzmeister, F., Camerer, C., Dreber, A., Huber, J., Johannesson, M., ... Schonberg, T. (2020). Variability in the analysis of a single neuroimaging dataset by many teams. *Nature*, 582(7810), 84–88. https://doi.org/10.1038/s41586-020-2314-9, PubMed: 32483374

Boubela, R., Kalcher, K., Huf, W., Kronnerwetter, C., Filzmoser, P., & Moser, E. (2013). Beyond noise: Using temporal ICA to extract meaningful information from high-frequency fMRI signal fluctuations during rest. *Frontiers in Human Neuroscience*, 7, 168. https://doi.org/10.3389/fnhum.2013.00168, PubMed: 23641208

Bouttier, J., Di Francesco, P., & Guitter, E. (2003). Geodesic distance in planar graphs. *Nuclear Physics B*, 663(3), 535–567. https://doi.org/10.1016/S0550-3213(03)00355-9

Braun, U., Plichta, M., Esslinger, C., Sauer, C., Haddad, L., Grimm, O., ... Meyer-Lindenberg, A. (2012). Test-retest reliability of resting-state connectivity network characteristics using fMRI and graph theoretical measures. *NeuroImage*, 59(2), 1404–1412. https://doi.org/10.1016/j.neuroimage.2011.08.044, PubMed: 21888983

Bridgeford, E., Wang, S., Wang, Z., Xu, T., Craddock, C., Dey, J., ... Vogelstein, J. (2021). Eliminating accidental deviations to minimize generalization error and maximize replicability: Applications in connectomics and genomics. *PLoS Computational Biology*, 17(9), e1009279. https://doi.org/10.1371/journal.pcbi.1009279, PubMed: 34529652

Bryce, N., Flournoy, J., Guassi Moreira, J., Rosen, M., Sambook, K., Mair, P., & McLaughlin, K. (2021). Brain parcellation selection: An overlooked decision point with meaningful effects on individual differences in resting-state functional connectivity. *NeuroImage*, 243, 118487. https://doi.org/10.1016/j.neuroimage.2021.118487, PubMed: 34419594

Bujang, M., & Baharum, N. (2017). A simplified guide to determination of sample size requirements for estimating the value of intraclass correlation coefficient: A review. *Archives of Orofacial Sciences*, 12(1), 1–11.

Bullmore, E., & Sporns, O. (2012). The economy of brain network organization. *Nature Reviews Neuroscience*, 13(5), 336–349. https://doi.org/10.1038/nrn3214, PubMed: 22498897

Buzsáki, G., & Draguhn, A. (2004). Neuronal oscillations in cortical networks. *Science*, 304(5679), 1926–1929. https://doi.org/10.1126/science.1099745, PubMed: 15218136

Buzsáki, G. (2009). *Rhythms of the brain.* Oxford University Press.

Chen, C.-H., Fiecas, M., Gutiérrez, E., Panizzon, M., Eyler, L., Vuoksimaa, E., ... Kremen, W. (2013). Genetic topography of brain morphology. *Proceedings of the National Academy of Sciences*, 110(42), 17089–17094. https://doi.org/10.1073/pnas.1308091110, PubMed: 24082094

Christensen, A., Kenett, Y., Aste, T., Silvia, P., & Kwapil, T. (2018). Network structure of the wisconsin schizotypy scales-short forms: Examining psychometric network filtering approaches. *Behavior Research Methods*, 50(6), 2531–2550. https://doi.org/10.3758/s13428-018-1032-9, PubMed: 29520631

Coalson, T., Van Essen, D., & Glasser, M. (2018). The impact of traditional neuroimaging methods on the spatial localization of cortical areas. *Proceedings of the National Academy of Sciences*, 115(27), E6356–E6365. https://doi.org/10.1073/pnas.1801582115, PubMed: 29925602

Cole, M. W., Bassett, D. S., Power, J. D., Braver, T. S., & Petersen, S. E. (2014). Intrinsic and task-evoked network architectures of the human brain. *Neuron*, 83(1), 238–251. https://doi.org/10.1016/j.neuron.2014.05.014, PubMed: 24991964

Cole, M. W., Ito, T., Bassett, D. S., & Schultz, D. H. (2016). Activity flow over resting-state networks shapes cognitive task activations. *Nature Neuroscience*, 19(12), 1718–1726. https://doi.org/10.1038/nn.4406, PubMed: 27723746

Cole, M. W., Reynolds, J. R., Power, J. D., Repovs, G., Anticevic, A., & Braver, T. S. (2013). Multi-task connectivity reveals flexible hubs for adaptive task control. *Nature Neuroscience*, 16(9), 1348–1355. https://doi.org/10.1038/nn.3470, PubMed: 23892552

Cordes, D., Haughton, V., Arfanakis, K., Carew, J., Turski, P., Moritz, C., ... Meyerand, M. (2001). Frequencies contributing to functional connectivity in the cerebral cortex in "resting-state" data. *American Journal of Neuroradiology*, *22*(7), 1326–1333. PubMed: 11498421

Craddock, R., Jbabdi, S., Yan, C.-G., Vogelstein, J., Castellanos, F., Di Martino, A., ... Milham, M. (2013). Imaging human connectomes at the macroscale. *Nature Methods*, *10*(6), 524–539. https://doi.org/10.1038/nmeth.2482, PubMed: 23722212

Desikan, R., Ségonne, F., Fischl, B., Quinn, B., Dickerson, B., Blacker, D., ... Killiany, R. (2006). An automated labeling system for subdividing the human cerebral cortex on MRI scans into gyral based regions of interest. *NeuroImage*, *31*(3), 968–980. https://doi.org/10.1016/j.neuroimage.2006.01.021, PubMed: 16530430

De Vico Fallani, F., Latora, V., & Chavez, M. (2017). A topological criterion for filtering information in complex brain networks. *PLoS Computational Biology*, *13*(1), e1005305. https://doi.org/10.1371/journal.pcbi.1005305, PubMed: 28076353

Dimitriadis, S., Antonakakis, M., Simos, P., Fletcher, J., & Papanicolaou, A. (2017). Data-driven topological filtering based on orthogonal minimal spanning trees: Application to multigroup magnetoencephalography resting-state connectivity. *Brain Connectivity*, *7*(10), 661–670. https://doi.org/10.1089/brain.2017.0512, PubMed: 28891322

Dimitriadis, S. I., Laskaris, N. A., Del Rio-Portilla, Y., & Koudounis, G. C. (2009). Characterizing dynamic functional connectivity across sleep stages from EEG. *Brain Topography*, *22*(2), 119–133. https://doi.org/10.1007/s10548-008-0071-4, PubMed: 19005749

Dubois, J., & Adolphs, R. (2016). Building a science of individual differences from fMRI. *Trends in Cognitive Sciences*, *20*(6), 425–443. https://doi.org/10.1016/j.tics.2016.03.014, PubMed: 27138646

Eickhoff, S. B., Milham, M., & Vanderwal, T. (2020). Towards clinical applications of movie fMRI. *NeuroImage*, *217*, 116860. https://doi.org/10.1016/j.neuroimage.2020.116860, PubMed: 32376301

Elliott, M., Knodt, A., Caspi, A., Moffitt, T., & Hariri, A. (2021a). Need for psychometric theory in neuroscience research and training: Reply to Kragel et al. (2021). *Psychological Science*, *32*(4), 627–629. https://doi.org/10.1177/0956797621996665, PubMed: 33685291

Elliott, M., Knodt, A., & Hariri, A. (2021b). Striving toward translation: Strategies for reliable fMRI measurement. *Trends in Cognitive Sciences*, *25*(9), 776–787. https://doi.org/10.1016/j.tics.2021.05.008, PubMed: 34134933

Esteban, O., Markiewicz, C., Blair, R., Moodie, C., Isik, A., Erramuzpe, A., ... Gorgolewski, K. (2019). fMRIPrep: A robust preprocessing pipeline for functional MRI. *Nature Methods*, *16*(1), 111–116. https://doi.org/10.1038/s41592-018-0235-4, PubMed: 30532080, PubMed: 16089598

Estrada, E., & Higham, D. J. (2010). Network properties revealed through matrix functions. *SIAM Review*, *52*(4), 696–714. https://doi.org/10.1137/090761070

Estrada, E., & Rodriguez-Velazquez, J. A. (2005). Subgraph centrality in complex networks. *Physical Review E*, *71*(5), 056103. https://doi.org/10.1103/PhysRevE.71.056103, PubMed: 16089598

Falk, E. B., Hyde, L. W., Mitchell, C., Faul, J., Gonzalez, R., Heitzeg, M. M., ... Schulenberg, J. (2013). What is a representative brain? Neuroscience meets population science. *Proceedings of the National Academy of Sciences*, *110*(44), 17615–17622. https://doi.org/10.1073/pnas.1310134110, PubMed: 24151336

Fan, L., Li, H., Zhuo, J., Zhang, Y., Wang, J., Chen, L., ... Jiang, T. (2016). The Human Brainnetome Atlas: A new brain atlas based on connectional architecture. *Cerebral Cortex*, *26*(8), 3508–3526. https://doi.org/10.1093/cercor/bhw157, PubMed: 27230218

Faskowitz, J., Esfahlani, F., Jo, Y., Sporns, O., & Betzel, R. (2020). Edge-centric functional network representations of human cerebral cortex reveal overlapping system-level architecture. *Nature Neuroscience*, *23*(12), 1644–1654. https://doi.org/10.1038/s41593-020-00719-y, PubMed: 33077948

Finn, E. (2021). Is it time to put rest to rest? *Trends in Cognitive Sciences*, *25*(12), 1021–1032. https://doi.org/10.1016/j.tics.2021.09.005, PubMed: 34625348

Finn, E., Glerean, E., Hasson, U., & Vanderwal, T. (2022). Naturalistic imaging: The use of ecologically valid conditions to study brain function. *NeuroImage*, *247*, 118776. https://doi.org/10.1016/j.neuroimage.2021.118776, PubMed: 34864153

Finn, E., & Rosenberg, M. (2021). Beyond fingerprinting: Choosing predictive connectomes over reliable connectomes. *NeuroImage*, *239*, 118254. https://doi.org/10.1016/j.neuroimage.2021.118254, PubMed: 34118397

Fornito, A., Zalesky, A., & Breakspear, M. (2015). The connectomics of brain disorders. *Nature Reviews Neuroscience*, *16*(3), 159–172. https://doi.org/10.1038/nrn3901, PubMed: 25697159

Fox, M., & Raichle, M. (2007). Spontaneous fluctuations in brain activity observed with functional magnetic resonance imaging. *Nature Reviews Neuroscience*, *8*(9), 700–711. https://doi.org/10.1038/nrn2201, PubMed: 17704812

Freeman, L. C. (1978). Centrality in social networks conceptual clarification. *Social Networks*, *1*(3), 215–239. https://doi.org/10.1016/0378-8733(78)90021-7

Gao, J., Chen, G., Wu, J., Wang, Y., Hu, Y., Xu, T., ... Yang, Z. (2020). Reliability map of individual differences reflected in inter-subject correlation in naturalistic imaging. *NeuroImage*, *223*, 117277. https://doi.org/10.1016/j.neuroimage.2020.117277, PubMed: 32818614

Garrison, K. A., Scheinost, D., Finn, E. S., Shen, X., & Constable, R. T. (2015). The (in)stability of functional brain network measures across thresholds. *NeuroImage*, *118*, 651–661. https://doi.org/10.1016/j.neuroimage.2015.05.046, PubMed: 26021218

Ginestet, C. E., Nichols, T. E., Bullmore, E. T., & Simmons, A. (2011). Brain network analysis: Separating cost from topology using cost-integration. *PLoS One*, *6*(7), e21570. https://doi.org/10.1371/journal.pone.0021570, PubMed: 21829437

Giusti, C., Ghrist, R., & Bassett, D. S. (2016). Two's company, three (or more) is a simplex. *Journal of Computational Neuroscience*, *41*(1), 1–14. https://doi.org/10.1007/s10827-016-0608-6, PubMed: 27287487

Glasser, M., Coalson, T., Robinson, E., Hacker, C., Harwell, J., Yacoub, E., ... Van Essen, D. (2016). A multi-modal parcellation of human cerebral cortex. *Nature*, *536*(7615), 171–178. https://doi.org/10.1038/nature18933, PubMed: 27437579

Glasser, M., Sotiropoulos, S., Wilson, J., Coalson, T., Fischl, B., Andersson, J., ... Jenkinson, M. (2013). The minimal preprocessing pipelines for the Human Connectome Project. *NeuroImage*, *80*, 105–124. https://doi.org/10.1016/j.neuroimage.2013.04.127, PubMed: 23668970

Gong, Z.-Q., Gao, P., Jiang, C., Xing, X.-X., Dong, H.-M., White, T., ... Zuo, X.-N. (2021). DREAM: A toolbox to decode rhythms of the brain system. *Neuroinformatics*, *19*(3), 529–545. https://doi.org/10.1007/s12021-020-09500-9, PubMed: 33409718

Gratton, C., Nelson, S., & Gordon, E. (2022). Brain-behavior correlations: Two paths toward reliability. *Neuron*, *110*(9), 1446–1449. https://doi.org/10.1016/j.neuron.2022.04.018, PubMed: 35512638

Greene, A. S., Shen, X., Noble, S., Horien, C., Hahn, C. A., Arora, J., ... Constable, R. T. (2022). Brain–phenotype models fail for individuals who defy sample stereotypes. *Nature*, *609*(7925), 109–118. https://doi.org/10.1038/s41586-022-05118-w, PubMed: 36002572

Greene, D., Marek, S., Gordon, E., Siegel, J., Gratton, C., Laumann, T., ... Dosenbach, N. (2020). Integrative and network-specific connectivity of the basal ganglia and thalamus defined in individuals. *Neuron*, *105*(4), 742–758. https://doi.org/10.1016/j.neuron.2019.11.012, PubMed: 31836321

Guo, H., Qin, M., Chen, J., Xu, Y., & Xiang, J. (2017). Machine-learning classifier for patients with major depressive disorder: Multifeature approach based on a high-order minimum spanning tree functional brain network. *Computational and Mathematical Methods in Medicine*, *2017*, 4820935. https://doi.org/10.1155/2017/4820935, PubMed: 29387141

Hagmann, P., Kurant, M., Gigandet, X., Thiran, P., Wedeen, V., Meuli, R., & Thiran, J.-P. (2007). Mapping human whole-brain structural networks with diffusion MRI. *PLoS One*, *2*(7), e597. https://doi.org/10.1371/journal.pone.0000597, PubMed: 17611629

Hallquist, M. N., & Hillary, F. G. (2019). Graph theory approaches to functional network organization in brain disorders: A critique for a brave new small-world. *Network Neuroscience*, *3*(1), 1–26. https://doi.org/10.1162/netn_a_00054, PubMed: 30793071

Helwegen, K., Libedinsky, I., & van den Heuvel, M. P. (2023). Statistical power in network neuroscience. *Trends in Cognitive Sciences*, *27*(3), 282–301 https://doi.org/10.1016/j.tics.2022.12.011, PubMed: 36725422

Herting, M., Gautam, P., Chen, Z., Mezher, A., & Vetter, N. (2018). Test-retest reliability of longitudinal task-based fMRI: Implications for developmental studies. *Developmental Cognitive Neuroscience*, *33*, 17–26. https://doi.org/10.1016/j.dcn.2017.07.001, PubMed: 29158072

Hilger, K., & Markett, S. (2021). Personality network neuroscience: Promises and challenges on the way toward a unifying framework of individual variability. *Network Neuroscience*, *5*(3), 631–645. https://doi.org/10.1162/netn_a_00198, PubMed: 34746620

Ji, J., Spronk, M., Kulkarni, K., Repovš, G., Anticevic, A., & Cole, M. (2019). Mapping the human brain's cortical-subcortical functional network organization. *NeuroImage*, *185*, 35–57. https://doi.org/10.1016/j.neuroimage.2018.10.006, PubMed: 30291974

Kardan, O., Stier, A. J., Cardenas-Iniguez, C., Schertz, K. E., Pruin, J. C., Deng, Y., ... Rosenberg, M. D. (2022). Differences in the functional brain architecture of sustained attention and working memory in youth and adults. *PLoS Biology*, *20*(12), e3001938. https://doi.org/10.1371/journal.pbio.3001938, PubMed: 36542658

Koo, T., & Li, M. (2016). A guideline of selecting and reporting intraclass correlation coefficients for reliability research. *Journal of Chiropractic Medicine*, *15*(2), 155–163. https://doi.org/10.1016/j.jcm.2016.02.012, PubMed: 27330520

Kraemer, H. (2014). The reliability of clinical diagnoses: State of the art. *Annual Review of Clinical Psychology, 10*, 111–130. https://doi.org/10.1146/annurev-clinpsy-032813-153739, PubMed: 24387235

Latora, V., & Marchiori, M. (2001). Efficient behavior of small-world networks. *Physical Review Letters*, *87*(19), 198701. https://doi.org/10.1103/PhysRevLett.87.198701, PubMed: 11690461

Li, X., Ai, L., Giavasis, S., Jin, H., Feczko, E., Xu, T., ... Milham, M. P. (2022). Moving beyond processing and analysis-related variation in neuroscience. *bioRxiv*. https://doi.org/10.1101/2021.12.01.470790

Liang, X., Wang, J., Yan, C., Shu, N., Xu, K., Gong, G., & He, Y. (2012). Effects of different correlation metrics and preprocessing factors on small-world brain functional networks: A resting-state functional MRI study. *PLoS One*, *7*(3), e32766. https://doi.org/10.1371/journal.pone.0032766, PubMed: 22412922

Mantegna, R. (1999). Hierarchical structure in financial markets. *European Physical Journal B*, *11*(1), 193–197. https://doi.org/10.1007/s100510050929

Marek, S., Siegel, J., Gordon, E., Raut, R., Gratton, C., Newbold, D., ... Dosenbach, N. (2018). Spatial and temporal organization of the individual human cerebellum. *Neuron*, *100*(4), 977–993. https://doi.org/10.1016/j.neuron.2018.10.010, PubMed: 30473014

Marek, S., Tervo-Clemmens, B., Calabro, F., Montez, D., Kay, B., Hatoum, A., ... Dosenbach, N. (2022). Reproducible brain-wide association studies require thousands of individuals. *Nature*, *603*(7902), 654–660. https://doi.org/10.1038/s41586-022-04492-9, PubMed: 35296861

Massara, G., Di Matteo, T., & Aste, T. (2016). Network filtering for big data: Triangulated maximally filtered graph. *Journal of Complex Networks*, *5*(2), 161–178. https://doi.org/10.1093/comnet/cnw015

Matheson, G. (2019). We need to talk about reliability: Making better use of test-retest studies for study design and interpretation. *PeerJ*, *2019*(5), e6918. https://doi.org/10.7717/peerj.6918, PubMed: 31179173

Matthews, P., & Hampshire, A. (2016). Clinical concepts emerging from fMRI functional connectomics. *Neuron*, *91*(3), 511–528. https://doi.org/10.1016/j.neuron.2016.07.031, PubMed: 27497220

McCormick, E. M., Arnemann, K. L., Ito, T., Hanson, S. J., & Cole, M. W. (2022). Latent functional connectivity underlying multiple brain states. *Network Neuroscience*, *6*(2), 570–590. https://doi.org/10.1162/netn_a_00234, PubMed: 35733420

Meier, J., Tewarie, P., & Van Mieghem, P. (2015). The union of shortest path trees of functional brain networks. *Brain Connectivity*, *5*(9), 575–581. https://doi.org/10.1089/brain.2014.0330, PubMed: 26027712

Micheloyannis, S., Pachou, E., Stam, C. J., Breakspear, M., Bitsios, P., Vourkas, M., ... Zervakis, M. (2006). Small-world networks and disturbed functional connectivity in schizophrenia. *Schizophrenia Research*, *87*(1–3), 60–66. https://doi.org/10.1016/j.schres.2006.06.028, PubMed: 16875801

Milham, M., Vogelstein, J., & Xu, T. (2021). Removing the reliability bottleneck in functional magnetic resonance imaging research to

achieve clinical utility. *JAMA Psychiatry*, *78*(6), 587–588. https://doi.org/10.1001/jamapsychiatry.2020.4272, PubMed: 33439234

Milo, R., Shen-Orr, S., Itzkovitz, S., Kashtan, N., Chklovskii, D., & Alon, U. (2002). Network motifs: Simple building blocks of complex networks. *Science*, *298*(5594), 824–827. https://doi.org/10.1126/science.298.5594.824, PubMed: 12399590

Munafo, M., Nosek, B., Bishop, D., Button, K., Chambers, C., Percie Du Sert, N., ... Ioannidis, J. (2017). A manifesto for reproducible science. *Nature Human Behaviour*, *1*(1), 0021. https://doi.org/10.1038/s41562-016-0021, PubMed: 33954258

Newman, M. E. (2003). The structure and function of complex networks. *SIAM Review*, *45*(2), 167–256. https://doi.org/10.1137/S003614450342480

Newman, M. E. (2004). Fast algorithm for detecting community structure in networks. *Physical Review E*, *69*(6), 066133. https://doi.org/10.1103/PhysRevE.69.066133, PubMed: 15244693

Newman, M. E. (2008). The mathematics of networks. *The New Palgrave Encyclopedia of Economics*, *2*(2008), 1–12. https://doi.org/10.1057/978-1-349-95121-5_2565-1

Noble, S., Scheinost, D., & Todd Constable, R. (2019). A decade of test-retest reliability of functional connectivity: A systematic review and meta-analysis. *NeuroImage*, *203*, 116157. https://doi.org/10.1016/j.neuroimage.2019.116157, PubMed: 31494250

Noble, S., Scheinost, D., & Todd Constable, R. (2021). A guide to the measurement and interpretation of fmri test-retest reliability. *Current Opinion in Behavioral Sciences*, *40*, 27–32. https://doi.org/10.1016/j.cobeha.2020.12.012, PubMed: 33585666

Otte, W., van Diessen, E., Paul, S., Ramaswamy, R., Subramanyam Rallabandi, V., Stam, C., & Roy, P. (2015). Aging alterations in whole-brain networks during adulthood mapped with the minimum spanning tree indices: The interplay of density, connectivity cost and life-time trajectory. *NeuroImage*, *109*, 171–189. https://doi.org/10.1016/j.neuroimage.2015.01.011, PubMed: 25585021

Page, L., Brin, S., Motwani, R., & Winograd, T. (1999). *The PageRank citation ranking: Bringing order to the web* (Tech. Rep.). Stanford, California: Stanford InfoLab.

Pastor-Satorras, R., Vázquez, A., & Vespignani, A. (2001). Dynamical and correlation properties of the internet. *Physical Review Letters*, *87*(25), 258701. https://doi.org/10.1103/PhysRevLett.87.258701, PubMed: 11736611

Paus, T. (2010). Population neuroscience: Why and how. *Human Brain Mapping*, *31*(6), 891–903. https://doi.org/10.1002/hbm.21069, PubMed: 20496380

Penttonen, M., & Buzsáki, G. (2003). Natural logarithmic relationship between brain oscillators. *Thalamus and Related Systems*, *2*(2), 145–152. https://doi.org/10.1016/S1472-9288(03)00007-4

Pessoa, L. (2018). Understanding emotion with brain networks. *Current Opinion in Behavioral Sciences*, *19*, 19–25. https://doi.org/10.1016/j.cobeha.2017.09.005, PubMed: 29915794

Power, J. D., Mitra, A., Laumann, T. O., Snyder, A. Z., Schlaggar, B. L., & Petersen, S. E. (2014). Methods to detect, characterize, and remove motion artifact in resting state fMRI. *NeuroImage*, *84*(Suppl. C), 320–341. https://doi.org/10.1016/j.neuroimage.2013.08.048, PubMed: 23994314

Rakic, P. (2009). Evolution of the neocortex: A perspective from developmental biology. *Nature Reviews Neuroscience*, *10*(10), 724–735. https://doi.org/10.1038/nrn2719, PubMed: 19763105

Ricard, J., Parker, T., Dhamala, E., Kwasa, J., Allsop, A., & Holmes, A. (2023). Confronting racially exclusionary practices in the acquisition and analyses of neuroimaging data. *Nature Neuroscience*, *26*(1), 4–11. https://doi.org/10.1038/s41593-022-01218-y, PubMed: 36564545

Rosenberg, M. D., & Finn, E. S. (2022). How to establish robust brain-behavior relationships without thousands of individuals. *Nature Neuroscience*, *25*(7), 835–837. https://doi.org/10.1038/s41593-022-01110-9, PubMed: 35710985

Rubinov, M., & Sporns, O. (2010). Complex network measures of brain connectivity: Uses and interpretations. *NeuroImage*, *52*(3), 1059–1069. https://doi.org/10.1016/j.neuroimage.2009.10.003, PubMed: 19819337

Rubinov, M., Sporns, O., van Leeuwen, C., & Breakspear, M. (2009). Symbiotic relationship between brain structure and dynamics. *BMC Neuroscience*, *10*, 55. https://doi.org/10.1186/1471-2202-10-55, PubMed: 19486538

Salvador, R., Suckling, J., Coleman, M., Pickard, J., Menon, D., & Bullmore, E. (2005). Neurophysiological architecture of functional magnetic resonance images of human brain. *Cerebral Cortex*, *15*(9), 1332–1342. https://doi.org/10.1093/cercor/bhi016, PubMed: 15635061

Santarnecchi, E., Galli, G., Polizzotto, N., Rossi, A., & Rossi, S. (2014). Efficiency of weak brain connections support general cognitive functioning. *Human Brain Mapping*, *35*(9), 4566–4582. https://doi.org/10.1002/hbm.22495, PubMed: 24585433

Schaefer, A., Kong, R., Gordon, E., Laumann, T., Zuo, X.-N., Holmes, A., ... Yeo, B. (2018). Local-global parcellation of the human cerebral cortex from intrinsic functional connectivity MRI. *Cerebral Cortex*, *28*(9), 3095–3114. https://doi.org/10.1093/cercor/bhx179, PubMed: 28981612

Smith, S., Beckmann, C., Andersson, J., Auerbach, E., Bijsterbosch, J., Douaud, G., ... Glasser, M. (2013). Resting-state fMRI in the Human Connectome Project. *NeuroImage*, *80*, 144–168. https://doi.org/10.1016/j.neuroimage.2013.05.039, PubMed: 23702415

Song, W.-M., Di Matteo, T., & Aste, T. (2012). Hierarchical information clustering by means of topologically embedded graphs. *PLoS One*, *7*(3), e31929. https://doi.org/10.1371/journal.pone.0031929, PubMed: 22427814

Sporns, O. (2013a). Making sense of brain network data. *Nature Methods*, *10*(6), 491–493. https://doi.org/10.1038/nmeth.2485, PubMed: 23722207

Sporns, O. (2013b). Network attributes for segregation and integration in the human brain. *Current Opinion in Neurobiology*, *23*(2), 162–171. https://doi.org/10.1016/j.conb.2012.11.015, PubMed: 23294553

Stam, C., Jones, B., Nolte, G., Breakspear, M., & Scheltens, P. (2007). Small-world networks and functional connectivity in Alzheimer's disease. *Cerebral Cortex*, *17*(1), 92–99. https://doi.org/10.1093/cercor/bhj127, PubMed: 16452642

Termenon, M., Jaillard, A., Delon-Martin, C., & Achard, S. (2016). Reliability of graph analysis of resting state fMRI using test-retest dataset from the Human Connectome Project. *NeuroImage*, *142*, 172–187. https://doi.org/10.1016/j.neuroimage.2016.05.062, PubMed: 27282475

Thomas Yeo, B., Krienen, F., Sepulcre, J., Sabuncu, M., Lashkari, D., Hollinshead, M., ... Buckner, R. (2011). The organization of the human cerebral cortex estimated by intrinsic functional

connectivity. *Journal of Neurophysiology*, *106*(3), 1125–1165. https://doi.org/10.1152/jn.00338.2011, PubMed: 21653723

Tibon, R., Geerligs, L., & Campbell, K. (2022). Bridging the big (data) gap: Levels of control in small- and large-scale cognitive neuroscience research. *Trends in Neurosciences*, *45*(7), 507–516. https://doi.org/10.1016/j.tins.2022.03.011, PubMed: 35469691

Toi, P., Jang, H., Min, K., Kim, S.-P., Lee, S.-K., Lee, J., ... Park, J.-Y. (2022). In vivo direct imaging of neuronal activity at high temporospatial resolution. *Science*, *378*(6616), 160–168. https://doi.org/10.1126/science.abh4340, PubMed: 36227975

Tumminello, M., Aste, T., Di Matteo, T., & Mantegna, R. (2005). A tool for filtering information in complex systems. *Proceedings of the National Academy of Sciences*, *102*(30), 10421–10426. https://doi.org/10.1073/pnas.0500298102, PubMed: 16027373

van den Heuvel, M. P., de Lange, S. C., Zalesky, A., Seguin, C., Yeo, B. T., & Schmidt, R. (2017). Proportional thresholding in resting-state fMRI functional connectivity networks and consequences for patient-control connectome studies: Issues and recommendations. *NeuroImage*, *152*, 437–449. https://doi.org/10.1016/j.neuroimage.2017.02.005, PubMed: 28167349

van Nieuwenhuizen, D., Douw, L., Klein, M., Peerdeman, S., Heimans, J., Reijneveld, J., ... Hillebrand, A. (2018). Cognitive functioning and functional brain networks in postoperative WHO grade I meningioma patients. *Journal of Neuro-Oncology*, *140*(3), 605–613. https://doi.org/10.1007/s11060-018-2987-1, PubMed: 30219943

Wang, J., Wang, L., Zang, Y., Yang, H., Tang, H., Gong, Q., ... He, Y. (2009). Parcellation-dependent small-world brain functional networks: A resting-state fMRI study. *Human Brain Mapping*, *30*(5), 1511–1523. https://doi.org/10.1002/hbm.20623, PubMed: 18649353

Watts, D. J., & Strogatz, S. H. (1998). Collective dynamics of 'small-world' networks. *Nature*, *393*(6684), 440–442. https://doi.org/10.1038/30918, PubMed: 9623998

Xing, X.-X., Xu, T., Jiang, C., Wang, Y., & Zuo, X.-N. (2022). Connectome Computation System: 2015–2021 updates. *Science Bulletin*, *67*(5), 448–451. https://doi.org/10.1016/j.scib.2021.11.021, PubMed: 36546160

Xing, X.-X., & Zuo, X.-N. (2018). The anatomy of reliability: A must read for future human brain mapping. *Science Bulletin*, *63*(24), 1606–1607. https://doi.org/10.1016/j.scib.2018.12.010, PubMed: 36658850

Xu, T., Yang, Z., Jiang, L., Xing, X.-X., & Zuo, X.-N. (2015). A connectome computation system for discovery science of brain. *Science Bulletin*, *60*(1), 86–95. https://doi.org/10.1007/s11434-014-0698-3

Yarkoni, T. (2022). The generalizability crisis. *Behavioral and Brain Sciences*, *45*, e1. https://doi.org/10.1017/S0140525X20001685, PubMed: 33342451

Zalesky, A., Fornito, A., Harding, I., Cocchi, L., Yücel, M., Pantelis, C., & Bullmore, E. (2010). Whole-brain anatomical networks: Does the choice of nodes matter? *NeuroImage*, *50*(3), 970–983. https://doi.org/10.1016/j.neuroimage.2009.12.027, PubMed: 20035887

Zeng, L.-L., Wang, D., Fox, M., Sabuncu, M., Hu, D., Ge, M., ... Liu, H. (2014). Neurobiological basis of head motion in brain imaging. *Proceedings of the National Academy of Sciences*, *111*(16), 6058–6062. https://doi.org/10.1073/pnas.1317424111, PubMed: 24711399

Zhao, W., Makowski, C., Hagler, D. J., Garavan, H. P., Thompson, W. K., Greene, D. J., ... Dale, A. M. (2023). Task fMRI paradigms may capture more behaviorally relevant information than resting-state functional connectivity. *NeuroImage*, *270*, 119946. https://doi.org/10.1016/j.neuroimage.2023.119946, PubMed: 36801369

Zhou, Y., Chen, J., Luo, Y. L., Zheng, D., Rao, L.-L., Li, X., ... Zuo, X.-N. (2016). Genetic overlap between in-scanner head motion and the default network connectivity. *bioRxiv*. https://doi.org/10.1101/087023

Zuo, X.-N., Biswal, B., & Poldrack, R. (2019a). Editorial: Reliability and reproducibility in functional connectomics. *Frontiers in Neuroscience*, *13*, 117. https://doi.org/10.3389/fnins.2019.00117, PubMed: 30842722

Zuo, X. N., Di Martino, A., Kelly, C., Shehzad, Z. E., Gee, D. G., Klein, D. F., ... Milham, M. P. (2010). The oscillating brain: Complex and reliable. *NeuroImage*, *49*(2), 1432–1445. https://doi.org/10.1016/j.neuroimage.2009.09.037, PubMed: 19782143

Zuo, X.-N., He, Y., Betzel, R., Colcombe, S., Sporns, O., & Milham, M. (2017). Human connectomics across the life span. *Trends in Cognitive Sciences*, *21*(1), 32–45. https://doi.org/10.1016/j.tics.2016.10.005, PubMed: 27865786

Zuo, X.-N., He, Y., Su, X., Hou, X.-H., Weng, X., & Li, Q. (2018). Developmental population neuroscience: Emerging from ICHBD. *Science Bulletin*, *63*(6), 331–332. https://doi.org/10.1016/j.scib.2018.01.008, PubMed: 36658866

Zuo, X.-N., & Xing, X.-X. (2014). Test-retest reliabilities of resting-state FMRI measurements in human brain functional connectomics: A systems neuroscience perspective. *Neuroscience and Biobehavioral Reviews*, *45*, 100–118. https://doi.org/10.1016/j.neubiorev.2014.05.009, PubMed: 24875392

Zuo, X.-N., Xu, T., Jiang, L., Yang, Z., Cao, X.-Y., He, Y., ... Milham, M. (2013). Toward reliable characterization of functional homogeneity in the human brain: Preprocessing, scan duration, imaging resolution and computational space. *NeuroImage*, *65*, 374–386. https://doi.org/10.1016/j.neuroimage.2012.10.017, PubMed: 23085497

Zuo, X.-N., Xu, T., & Milham, M. (2019b). Harnessing reliability for neuroscience research. *Nature Human Behaviour*, *3*(8), 768–771. https://doi.org/10.1038/s41562-019-0655-x, PubMed: 31253883